ICARUS 100, 464–484 (1992)

New Observations of Saturn's Coorbital Satellites[1]

PHILIP D. NICHOLSON AND DOUGLAS P. HAMILTON

Astronomy Department, Cornell University, Ithaca, New York 14853

KEITH MATTHEWS

Palomar Observatory, California Institute of Technology, Pasadena, California 91125

AND

CHARLES F. YODER

Jet Propulsion Laboratory, California Institute of Technology, 4800 Oak Grove Avenue, Pasadena, California 91109

Received December 24, 1991; revised September 16, 1992

We present observations of the Saturnian coorbital satellites, Janus and Epimetheus, obtained with the Caltech Cassegrain infrared camera at the Palomar Hale telescope in July and August 1990. Exploiting the strong planetary methane and hydrogen absorption at $\lambda 2.0$–$2.4\ \mu$m, we observed both satellites as they passed over Saturn's north pole at superior conjunction. At that time, the bright rings were blocked or eclipsed by the planet, permitting observations of the much fainter satellites. The larger coorbital, Janus, was detected in a single image on 1 July and in seven images on 4 July. Epimetheus was first detected in four images on 4 July and subsequently in five images on 11–13 July and in seventeen images on 14 August 1990. Exposure times varied from 60 to 240 sec, and both narrowband (CVF) and broadband K filters were used. Astrometric reductions relative to the brighter satellites, chiefly Mimas and Enceladus, yield planetocentric positions of the coorbitals with accuracies of 0.15–0.35″, or 0.4°–0.9° in longitude. These measurements are combined with Voyager and previous Earth-based observations made in 1980–1981 and the discovery observations in 1966, in a revised solution for the dynamical parameters of the system. The orbital model is that of Yoder *et al.* (1989, *Astron. J.* 98, 1875–1889). Our new observations confirm their results, in particular the low densities of both satellites, but provide a much stronger solution which is essentially independent of lingering uncertainties in the interpretation of the 1966 data for Epimetheus. We obtain masses of $(1.98 \pm 0.12) \times 10^{21}$ g for Janus, and $(0.55 \pm 0.03) \times 10^{21}$ g for Epimetheus which, together with the volume estimates by Thomas (1989, *Icarus* 77, 248–274) and Yoder *et al.* (1989) based on Voyager images, yield mean densities of 0.65 ± 0.08 and 0.63 ± 0.11 g cm^{-3}, respectively. Similar densities for these bodies have recently been derived by Rosen *et al.* (1991, *Icarus* 93, 25–44) from an analysis of density waves driven in Saturn's rings. The most natural interpretation of these densities is that these objects (whose mean radii are 90 and 59 km) are composed of relatively pure water ice, but with porosities of ~30%. A similar porosity has been inferred by Dermott and Thomas (1988, *Icarus* 73, 25–65) and Eluszkiewicz (1990, *Icarus* 84, 215–225) for the outer 50–70 km of the mantle of Mimas.

[1] The observations reported here were made as a part of a continuing collaborative agreement between the California Institute of Technology and Cornell University.

1. INTRODUCTION

1.1. Dynamics

Janus and Epimetheus, commonly referred to as the coorbital satellites of Saturn, move on nearly identical, low-eccentricity orbits just outside Saturn's main ring system. Slight differences in orbital mean motions cause the moons to approach one another at intervals of ~4 years, at which times their mutual gravitational attraction, normally negligible, is large enough to significantly alter their orbital motions. The resulting deviations from pure Keplerian motion contain information about the perturbing force and hence about the masses of the two moons. In fact, a complete set of orbital parameters can uniquely determine both satellites' masses (Yoder *et al.* 1983), a result that we attempt to motivate in the next few paragraphs.

Since the satellites are gravitationally influenced by one another as well as by Saturn, a three-body formalism is necessary to correctly treat their orbital motions. The appropriate solution for the motion of Janus and Epimetheus, as described by Dermott and Murray (1981) and

0019-1035/92 $5.00

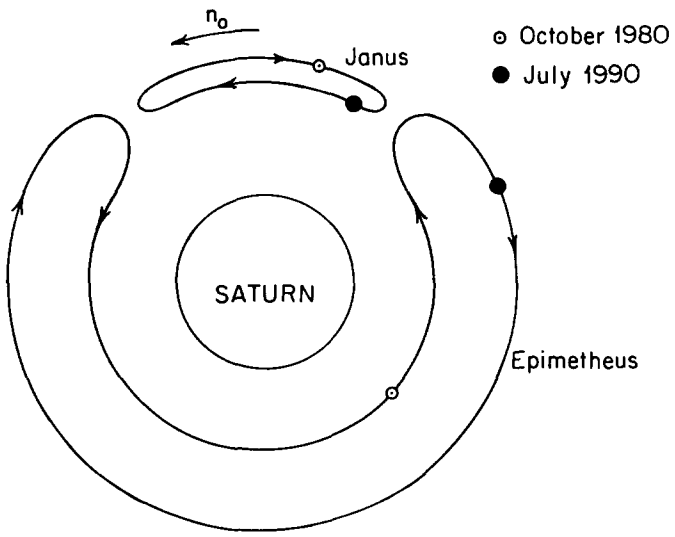

FIG. 1. The horseshoe orbit of Janus and Epimetheus, as seen in a reference frame rotating counterclockwise at the mean orbital angular velocity, n_0. The positions of both satellites in October 1980 (Voyager 1 encounter) and July 1990 (near the time of the Palomar observations) are indicated by open and filled circles, respectively. These two epochs are separated by just over one complete libration cycle of 2927 days. Arrows indicate the direction of librational motion. Note that the effects of orbital eccentricity on the satellite positions have been ignored in this figure: only radial excursions from the mean orbit due to the 1 : 1 resonance have been included and are exaggerated by a factor of 600. The true radial deviations are ±10 km for Janus and ±40 km for Epimetheus, less than the satellites' mean radii of 90 and 59 km.

Yoder *et al.* (1983), is analogous to the well-known stable libration of a test particle about the triangular Lagrange points exhibited by the classical restricted three-body problem, with the added complication that the masses of the two smaller bodies are comparable. The satellites move on horseshoe-shaped orbits when viewed in a reference frame rotating at the mass-weighted average mean motion of the two satellites, as illustrated in Fig. 1. Epimetheus orbits clockwise around the large horseshoe while Janus moves in the same direction around the smaller banana-shaped orbit at the top of the diagram. The dynamics of this motion can be understood qualitatively by following the moons through one libration period.

In October 1980, the satellites were in the positions indicated by the open circles in Fig. 1, with Epimetheus trailing Janus by ~110°; Epimetheus was then on the interior portion of its horseshoe traveling at a speed faster than the rate of rotation of the moving frame, while Janus, on the outer portion of its orbit, was traveling more slowly. Starting at this point in the libration cycle, the separation angle ϕ decreases nearly linearly with time, until the moons are sufficiently close for their gravitational interaction to become appreciable. Janus then pulls Epimetheus toward it, with the result that the smaller moon gains energy and moves up into the more distant part of its horseshoe orbit; simultaneously Epimetheus pulls Janus down into a closer orbit. Janus, now interior to Epimetheus and therefore moving faster, slowly draws away from the smaller moon and ϕ increases again. As the perturbation rapidly diminishes, the moons continue to orbit essentially independently until they meet again on the left-hand side of the diagram to reverse the above process, Epimetheus returning to the interior orbit and Janus to the outer.

The timescale for a complete libration around the horseshoe is 2927 days, or 8.01 years, during which time the moons each complete more than 4200 orbits around Saturn. The most recent close approach occurred around 22 January 1990; in early July 1990 the satellites were predicted to be separating, with $\phi \simeq 38°$. Figure 2 shows the calculated variation of ϕ, based on the dynamical solution presented in Section 5. Overplotted on the model are the observed separations summarized below, compressed into a single libration cycle in Fig. 2a and at their true dates in Fig. 2b. Note that the quasi-linear behavior of ϕ extends down to within ~50 days of closest approach, or $\phi \simeq 10°$. The average minimum angular separation is 5.6°, or ~14,900 km, much greater than the average radial distance between the two satellites' orbits of ~50 km. The true separation in both radius and longitude is also influenced by the satellites' eccentricities, $e_1 = 0.0067$ (Janus) and $e_2 = 0.0099$ (Epimetheus). In the extreme case of antialigned pericenters at the time of closest approach, these eccentricities will lead to periodic variations in the longitudinal separation of $\pm 2a(e_1 + e_2) \simeq \pm 5100$ km over each orbital period of 16.7 hr, where $a = 151{,}450$ km is the mean semimajor axis. However, the satellites remain within 1° of minimum separation for about 35 days or 50 orbital periods, ensuring that the mutual interaction over this period is well approximated by the average potential.

The ratios of the changes in both the semimajor axes and the mean motions suffered by the satellites during times of close approach are proportional to their mass ratio (Yoder *et al.* 1983) as can be understood by a consideration of angular momentum conservation or of the difference in the accelerations experienced by the moons. An even more interesting parameter, however, is the total satellite mass M_t, since this can be combined with volume estimates derived from Voyager images to yield the satellites' mean density, which in turn contains clues about their composition and origin. Both the minimum angular separation and the libration period are primarily determined by the combined mass; a satellite pair with a smaller M_t would make a closer approach and hence have a longer libration period for a given initial separation in the semimajor axis, Δa. For the observed orbital separation ($\dot{\phi} = 0.25°$/day, corresponding to $\Delta a \simeq 50$ km), a reduction of

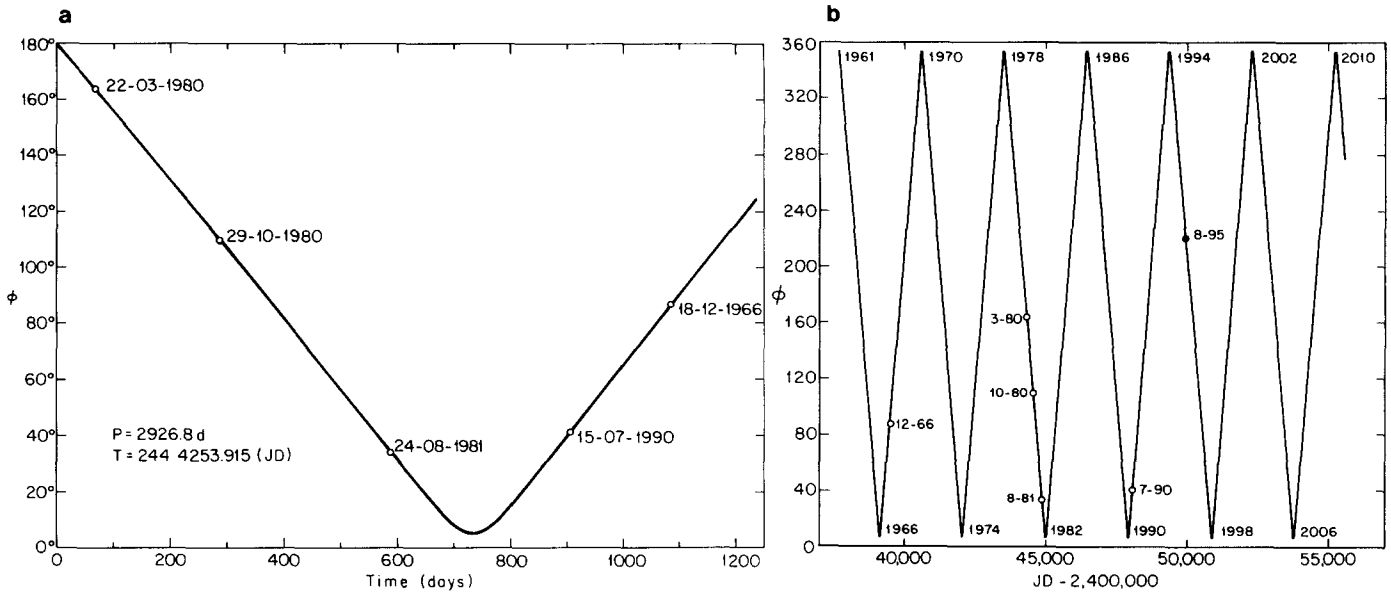

FIG. 2. (a) Variation of the longitude separation, $\phi = \lambda_J - \lambda_E$ with time during ~40% of a libration cycle, based on the dynamical model of Section 5. Corresponding numerical values of $\phi(t)$ for a quarter-cycle are given in Table VI. Also shown are the observed values of ϕ at the times of ring-plane crossing in December 1966 and March 1980, the Voyager encounters in October 1980 and August 1981, and the Palomar observations in July 1990. The mean satellite longitudes at these times are listed in Table IV. (b) Variation of ϕ over six libration periods between 1961 and 2010, based on the dynamical model of Section 5, showing the distribution of observations obtained between 1966 and 1990, as well as the predicted configurations at the next ring-plane crossing in August 1995 and during the era of anticipated Cassini observations in 2004–2008.

0.5 g cm^{-3} in the mean density results in a 1% (29 day) increase in the libration period (Yoder *et al.* 1983). The libration period, in turn, can be quite accurately determined from extended observations of ϕ spanning one or more close approaches.

Unfortunately, the highly accurate Voyager data and the best groundbased ring-plane crossing data were all obtained in the period 1980–1981, when the two moons were steadily approaching one another (see Fig. 2). In order to determine the total mass, therefore, it is necessary to combine the 1980–1981 data with observations made either prior to January 1978 or after January 1982, so that the overall data set spans at least one close approach. In the next section, we summarize published interpretations of the pre-1982 measurements before turning to a description of our 1990 observations in Sections 2 and 3 and a discussion of their implications for the satellite masses and densities in Sections 4 and 5.

1.2. Previous Observations

Under typical conditions of illumination, the intense scattered light from both the globe of Saturn and its rings makes observations of its small inner satellites extremely difficult with Earth-based telescopes. Only during brief periods when the Earth passes through the ring plane, or is on the opposite side of the rings from the Sun, is the scattered light from the rings sufficiently reduced to permit observations of these objects at visual wavelengths. The largest of Saturn's inner retinue, Janus (also designated S10 or 1966S1), was discovered by Dollfus (1967) on plates taken during the 1966 ring-plane crossing, although the initial orbit derived from these data proved to be erroneous. The existence of a second satellite, designated S11 or 1966S2, was subsequently inferred by Fountain and Larson (1977, 1978) from other plates taken in 1966, although Aksnes and Franklin (1978) disputed the validity of any particular orbit derived from these meager data.

Observations made during the ring-plane crossing of March 1980, followed up soon afterward by the encounters of Voyager 1 in November 1980 and Voyager 2 in August 1981, greatly clarified the situation (Seidelmann *et al.* 1981, Smith *et al.* 1981, 1982). The existence of two satellites in nearly identical orbits (1980S1 and 1980S3) was established, and a numerical study by Harrington and Seidelmann (1981) indicated that they participated in the horseshoe orbit libration described above, with a period of the order of 3000 days and a minimum separation of ~6°. The longitude separation, $\phi = \lambda_{S1} - \lambda_{S3}$, was found to be 172° on 12 March 1980 (Seidelmann *et al.* 1981) and 117° on 1 October 1980

near the time of the Voyager 1 encounter (Synnott *et al.* 1981; see also Fig. 2). The relative orbital motion, $\dot{\phi}$, was $-0.254°$/day in 1980–1981, with the next close approach predicted to occur in early 1982.

In a reevaluation of the 1966 observations, Larson *et al.* (1981) obtained an orbital period for S10 slightly less than that of 1980S1 and estimated that $\phi = 137°$ on 18 December 1966. In the process of this study, however, many of the putative S11 observations originally reported were reidentified with S10, and only three apparently genuine observations of S11 by Walker (1967) remained from the 1966 apparition (all, rather ironically, had been originally identified as S10). It could not be determined with certainty whether the satellites were approaching or separating in December 1966.

In the first attempt to link the 1966 and 1980 observations using an analytical model of the libration, Yoder *et al.* (1983) showed that the coorbitals must have been receding from one another in December 1966, and that the maximum value of ϕ at that time compatible with plausible satellite densities was ~90°. They proposed an alternative interpretation of the crucial 1966 S11 observations by Walker (1967), compatible with the dynamical model, for which $\phi \simeq 80°$. (Edge-on observations of satellite orbits inevitably lead to a far-side/near-side ambiguity unless the motion of the satellite is detected.) Based on these studies, and on the relative brightness of the two satellites, Janus = S10 was securely identified with 1980S1, and S11 with 1980S3, subsequently named Epimetheus.

In addition to the coorbital satellites, Voyager images revealed the presence of the F-ring shepherd satellites, Prometheus (1980S26) and Pandora (1980S27), and the much smaller Atlas (1980S28) near the outer edge of the A ring. Unfortunately, the similar brightnesses and orbital periods of Epimetheus, Pandora, and Prometheus led to some difficulties in identification even in 1980 and to more serious ambiguities in attempts to reassess the 1966 observations. In particular, the three remaining 1966 observations attributed to S11 by Larson *et al.* (1981) were also found by Yoder *et al.* (1989) to match the predicted positions of Prometheus. On the assumption, supported by a reinvestigation of the images obtained by Walker (1967), that both Prometheus and Epimetheus were visible in close proximity on 18 December 1966, Yoder *et al.* (1989) obtained a libration period of 2928.6 days, a minimum separation of 5.75°, and a remarkably low mean satellite density of 0.66 ± 0.10 g/cm^3.

As the putative 1966 observation of Epimetheus was crucial to the successful determination of the combined mass of the coorbital satellites, however, the unfortunate juxtaposition of Epimetheus and Prometheus cast some doubt on the orbit solution of Yoder *et al.* (1989), a doubt that could be removed only by additional observations of Epimetheus, and preferably of both satellites at a single epoch.

2. OBSERVATIONS

2.1. Observing Strategy

Given the obvious interest in confirming or refuting the unusually low mean density derived by Yoder *et al.* (1989), and knowing that the next ring-plane crossing will not occur until 1995, we sought a way to observe the satellites with the rings fully open. By observing at near-infrared wavelengths, especially in the 2.0- to 2.4-μm region, the scattered light from Saturn is greatly reduced by atmospheric methane and molecular hydrogen absorption. This approach has permitted imaging of the Uranian rings (Matthews *et al.* 1982, Allen 1983, Nicholson 1984), as well as the first groundbased observations of the small Jovian satellites, Metis and Adrastea (Nicholson and Matthews 1991). Saturn's rings, however, remain bright in this spectral region. Observations in the 3- to 4-μm range show the rings to be much fainter there, due to the fundamental water ice absorption at ~3.0 μm (Puetter and Russell 1977), but the steeply increasing terrestrial thermal background longward of 3.0 μm, combined with the probability that the satellites are spectrally similar to the icy rings, made it unlikely that we could detect the coorbitals at these wavelengths.

Our solution to this dilemma was to use the disk of Saturn to occult the bright rings and observe the satellites as they passed through superior conjunction, rather than at eastern or western elongation. An examination of the ring/satellite geometry indicated that, for a period of about 6 months in mid-1990, the ring-opening angle would be such as to fully block the A ring, while leaving the coorbital satellites continuously visible as they passed over Saturn's north pole. This fortuitous geometry is apparent in Fig. 3, a mosaic of Saturn and its rings at a wavelength of 2.2 μm obtained on 3 July 1990. Clearly shown here is the narrow gap in which we hoped to observe the satellites. Such a situation occurs only on four occasions during Saturn's 29-year orbital period, approximately 5 and 10 years after each ring-plane crossing, when the ring-opening angle is in the narrow range $21.4° < B < 23.9°$. In 1990, the relative positions of the Earth, Saturn, and the Sun restricted the useful window to just three months. In the future, successful observations of the coorbital satellites might also be made by employing the techniques of active optics to improve the atmospheric "seeing," or possibly with an optimized near-infrared filter at a high-altitude observatory such as Mauna Kea, although it is likely that the satellites are spectrally similar to the rings, as noted above.

Additional virtues of observations at superior conjunction with the rings fully open include a greatly enhanced

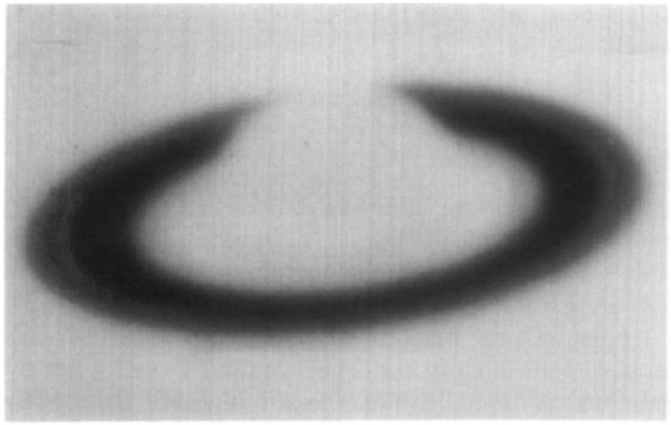

FIG. 3. A mosaic of nine individual IR camera frames of Saturn obtained on 3 July 1990 at a wavelength of 2.2 μm. Exposure time per image was 0.10 sec, and bad pixels have been replaced by interpolation from other images in the mosaic (a single unidentified bad pixel remains visible, repeated in each frame). Note the total obscuration of the rings at the planet's north pole, the key to successful infrared observations of the coorbital satellites at this epoch. (Image processing by S. Leroy.)

sensitivity of the measured positions to orbital longitude compared with observations at elongation, as well as the absence of the near-side/far-side ambiguity which afflicts all observations near elongation when the rings are presented edge on.

The ring–satellite geometry on the two nights on which the majority of our observations were obtained is illustrated in Figs. 4a and 4b; in the first of these the field of view of a single IR frame is also indicated as an aid to the interpretation of the images presented below. In early July 1990, near Saturn's opposition, the coorbital satellites approached to within ~0.5″ of Saturn's north pole at superior conjunction, and were expected to be visible for at most 30 min on each orbit. By August, the minimum separation had increased to ~0.9″, but the extent of blockage of the A ring was reduced markedly. Fortunately, the latter effect was offset by the increasing phase angle and resulting visibility of the planet's shadow across the rings, and the period of observability was again expected to be approximately 30 min per orbit.

Using positions of the coorbital satellites derived from the dynamical model of Yoder *et al.* (1989), we planned our observations to coincide with the predicted times of superior conjunction, allowing a ±30-min safety margin for the worst-case ephemeris errors. The predicted separation of $\phi = 38°$ on 4 July 1990 implied that Epimetheus would follow Janus by approximately 1 hr 45 min. Because of the 16.67-hr orbital period, opportunities for observation recur approximately every three orbits or 2 days. The calculated times (UT) of superior conjunction for the coorbital satellites and the F-ring shepherds on each night of successful observations were as follows. Saturn tran-

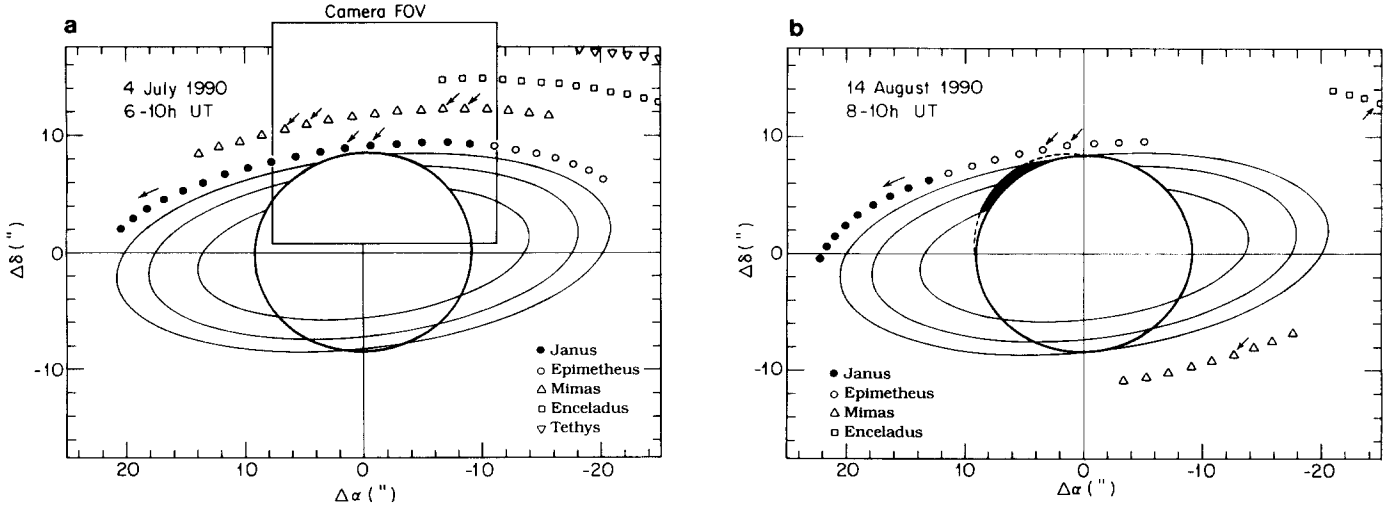

FIG. 4. (a) Saturn, its major ring components, and its inner satellites as observed on 4 July 1990, 10 days before opposition. The boundaries of the A and B rings are shown, and the projected oblateness of Saturn's disk is included. Positions of Janus, Epimetheus, Mimas, Enceladus, and Tethys are plotted at 15-min intervals between 6:00 and 10:00 UTC. Arrows indicate the approximate intervals during which the coorbital satellites were observable on this date, and the corresponding positions of Mimas. Janus was predicted to be at conjunction at 7:12 UT, and Epimetheus at 8:57 UT. A box indicates the 18″ × 19″ field of view of the IR camera. (b) The Saturn system on 14 August 1990, four weeks after opposition. The shadow of the planet on the rings is also indicated. Arrows indicate the approximate interval during which Epimetheus was observable on this date, and the positions at which Mimas and Enceladus were imaged to provide astrometric references (see text). Epimetheus was predicted to be at conjunction at 8:43 UT. All satellite positions are shown at 15-min intervals, between 8:00 and 10:00 UTC. Janus was not observed on this date, having passed superior conjunction at 6:30 UT.

sited at Palomar at ~8^{hr} UT in early July, and at ~5^{hr} UT in mid-August.

Date	Janus	Epimetheus	Prometheus	Pandora
1 July 1990	12:32.5	14:15.4	7:09.3	15:31.9
4 July 1990	7:12.3	8:57.2	8:42.2	3:51.6
11 July 1990	5:51.9	7:41.7	2:30.7	1:45.8
13 July 1990	7:51.8	9:43.0	13:21.1	14:05.5
14 August 1990	6:29.9	8:43.5	10:15.5	0:11.8

An additional opportunity on 2 July was thwarted by clouds. Only on 4 July was there any possibility that either Prometheus or Pandora might be confused with Janus or Epimetheus as happened in December 1966. Calculations of the planetocentric positions of the F-ring shepherds, however, showed that they should have been occulted by Saturn's limb for 20–30 min around superior conjunction, and thus were very unlikely to be visible at all.

2.2. *The Palomar IR Data Set*

All of the observations presented here were obtained with the Cassegrain Infrared camera at the 5-m Hale Telescope at Palomar Observatory. The principal characteristics of this instrument are described by Nicholson and Matthews (1991), to which the reader is referred for details. The image scale is 0.313″ per pixel, resulting in a field of view for the 58 × 62 pixel images of 18.2″ × 19.4″. The instrument is equipped with a circular variable filter (CVF) with a passband $\delta\lambda/\lambda = 0.013$ installed in one of the camera's two filter wheels, making it possible to select arbitrary wavelengths for observation in the range 1.8–2.6 μm. Standard broadband *JHKL* filters were installed in the other wheel.

Our several sets of observations between 1 July and 14 August 1990 are summarized in Table I. On each night, the telescope pointing was controlled by an automatic offset guider, set to track the satellite Titan. In this way, the geocentric motion of Saturn and its satellites was approximately removed. For exposures longer than 120 sec, however, the differential motion of Janus or Epimetheus relative to Titan exceeded 1 pixel. In such cases (except on 1 July, when no corrections were made), the offset guider was programmed to step in increments of ≥0.1″ at intervals of 1 min, so as to maintain a fixed camera pointing relative to the target satellite. Comparisons of Mimas images at the start and end of one 30-min run showed that this procedure worked extremely well, with no discernable displacement of the satellite's image on the array.

We now discuss briefly each of the nights on which observations were obtained.

TABLE I
Log of Observations

Date (1990)	UT range	No. of frames[a]	Exp. time (sec)	λ (μm)	⟨Airmass⟩	Satellite[b]
1 July	11:52–12:27	5(1)	240	2.10	3.48	Ja
4 July	6:51–7:34	19(7)	120	2.30	1.93	Ja
	8:17–9:57	22(4)	240	2.30	1.74	Ep
11 July	7:18–8:44	19(2)	240	2.30	1.74	Ep
13 July	8:34–10:37	18(3)	240	2.30	1.99	Ep
14 Aug.	8:18–8:48	26(17)	60	K[c]	3.05	Ep

[a] Number of coorbital satellite images in parentheses.
[b] Ja = Janus, Ep = Epimetheus.
[c] 2.0- to 2.4-μm passband.

2.2.1. 1 July observations. In our attempts to minimize the scattered light from both the planet and the rings, observations were initially made on 1 July using the CVF at a wavelength of 2.10 μm, where H_2 absorbs strongly in Saturn's atmosphere and where the wings of the water-ice band at 2.0 μm might at least partially suppress the ring brightness. Out of a series of five 240-sec exposures, taken shortly before sunrise at a very high airmass, Janus was faintly detected in the last frame as it approached superior conjunction. Mimas also appeared in these frames and could be used as an astrometric reference. Further observations were frustrated by morning twilight. Despite the ice absorption, the rings were found to be saturated in these exposures. Nevertheless, this initial success confirmed the accuracy of the Janus ephemeris and enabled us to refine our observational technique.

2.2.2. 4 July observations. As a result of the ring saturation at 2.10 μm, on 4 July we switched to a CVF wavelength of 2.30 μm, near the center of the planetary methane absorption, and abandoned further attempts to reduce the scattered ring flux. First Janus and then Epimetheus were imaged under ideal conditions near Saturn's transit at Palomar. Over a period of 40 min centered on Janus' predicted conjunction we obtained a series of nineteen 120-sec exposures. The satellite was visible in real-time displays of several images and subsequently was detected in a total of seven of these frames.

Starting 1 hr later, a series of twenty-two 240-sec exposures was taken to bracket the expected conjunction of Epimetheus. This was the first occasion on which we attempted to employ differential offset-guiding, in order to allow for the relative motion of Titan and the coorbital satellites. Although not visible in real-time inspection of the data, Epimetheus was detected in more carefully processed versions of four of these frames, very close to the predicted time of conjunction. Both Janus and Epimetheus images were framed so as to include Mimas as an astrometric reference (see Fig. 4a).

2.2.3. 11–13 July observations. Although the above observations established the viability of our observing

technique, we deemed it advisable to obtain additional observations of Epimetheus in particular, which is only faintly visible in the 4 July images. Opportunities arose to obtain the necessary follow-up data on 11 and 13 July, during other observing programs. On 11 July, nineteen 240-sec CVF exposures were obtained at 2.30 μm over a period of 90 min. Although Epimetheus appears clearly in only two frames (earlier frames in which it should have appeared were slightly out of focus), the seeing was excellent and the satellite images are unmistakeable.

On 13 July, eighteen 240-sec CVF exposures at 2.30 μm were obtained over a 2-hr period, with Epimetheus appearing clearly in three frames as it moved across the gap in scattered light from the rings. Unfortunately, no other satellites were available as nearby astrometric references, and these data are given correspondingly low weight in our orbit solution.

Several test images were also obtained on 13 July using a broadband K filter, rather than the CVF, with 10-sec exposure times. With a passband of 2.0–2.4 μm, this filter encompasses the entire planetary hydrogen/methane absorption band at 2.1–2.4 μm, as well as a continuum region shortward of 2.10 μm (Fink and Larson 1979). The measured throughput of this filter for a spectrally neutral source is ~12 times that of the narrowband CVF, which permits substantially shorter exposure times and thus more images per conjunction. These tests indicated that 30- to 60-sec exposures at K might yield better signal-to-noise ratios than the longer CVF exposures, despite a substantial increase in the scattered planetary flux.

2.2.4. 14 August observations. On 14 August we obtained twenty-six 60-sec exposures[2] using the K filter, over a period of 30 min around the predicted time of conjunction for Epimetheus. With the greater frame rate, we were successful in capturing Epimetheus in 17 of these frames. The image quality is generally superior to that of the narrowband exposures, although the scattered planetary flux is much more severe, as anticipated.

Although again no suitable reference satellite fell within our field of view on this night, we were able to establish an indirect astrometric reference by using the computer-controlled guider to offset the telescope in a precisely known manner and image Enceladus, Mimas, Tethys, and Rhea in turn. Throughout these observations, the guider tracked Titan continuously, providing a link between the Epimetheus images and those of the reference satellites.

[2] To avoid background saturation of the array, each frame actually consisted of four co-added 15-sec exposures.

3. DATA REDUCTION

3.1. Image Processing

Although the flux detected from Saturn, its rings, and the satellites is dominated by reflected sunlight in the near-infrared (for $\lambda \lesssim 4.5$ μm), there is a substantial terrestrial thermal background signal from the telescope and the atmosphere, as well as airglow emission, within the K band. This background signal, typically much larger than that from the faint objects of interest, was generally subtracted using single sky exposures taken immediately prior to or following the Saturn frames. The sky-subtracted frames were then flattened (i.e., corrected for pixel-to-pixel sensitivity variations) using exposures of the twilight sky from which appropriate dark-current frames had been subtracted to remove electronic offsets. In order to maximize our on-target time, and because of initial uncertainties in the ephemeris predictions, for the July observations we chose to obtain sky exposures by offsetting the telescope only 5″, or one-quarter of a frame width, to the north from our object frames. In this way it was possible to identify the satellite of interest in sky frames as well as in object frames. Although this procedure was successful, it results in a second, negative image of the rings appearing at the southern edge of our sky-subtracted images. (In all pictures presented in this paper, the 'positive' image is black, and the subtracted or 'negative' image is white, as in a photographic negative.)

The best sky-subtracted image of Janus from 4 July is shown in Fig. 5. The satellite is visible, albeit faintly, near the center of the gap in scattered light from the rings and just off Saturn's barely visible northern limb, while much brighter Mimas is immersed in scattered ring light near the western edge of the frame. Both satellites are indicated by vertical tick marks in the figure. The Janus image is ~3 pixels or 1″ in diameter; individual bright or dark pixels represent "bad" elements in the array. In the case of this frame, a second, negative image of Janus is also visible near the southern edge of the picture, due to the subtracted sky frame. The difficulties inherent in detecting small satellites in the vicinity of Saturn's bright rings are apparent in Fig. 5. The long exposure times necessary for the detection of such faint objects greatly increase the level of scattered light due to the telescope and the Earth's atmosphere, as is apparent in a comparison of Figs. 3 and 5. Even when they fall near the center of the gap in scattered light from the rings, as in Fig. 5, the coorbital satellites are difficult to detect in simple sky-subtracted images. Furthermore, the presence of strong local gradients in the scattered light background would be likely to systematically bias measurements of the satellite positions. We therefore experimented with several methods of subtracting the scattered light from the rings.

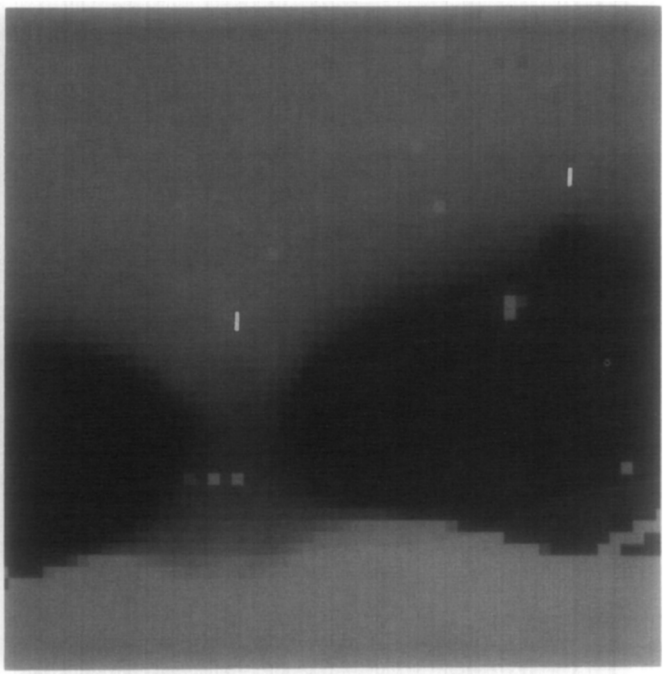

FIG. 5. A sky-subtracted and flat-fielded IR image of Janus obtained on 4 July 1990 at a wavelength of 2.30 μm (image 643). North is up, east is to the left. The camera field of view is illustrated in Fig. 4a. A similar image taken at a position offset 5″ to the north was used for sky subtraction, resulting in both positive (black) and negative (white) images of the rings in the lower part of the frame. The images of Janus and Mimas are indicated by vertical tick marks: Janus is approximately centered in the gap in scattered light from the rings, while Mimas is immersed in scattered light near the right (western) edge of the frame. Both satellite images are ~3 pixels (1″) FWHM diameter.

The simplest approach is to difference two images taken close together in time and therefore likely to show nearly identical scattered light profiles. However, the noise level in the processed frame is increased by a factor of $\sqrt{2}$ by each subtraction process, reducing the signal-to-noise ratio of the satellite detection. In order to minimize the additional noise, we therefore tried omitting the initial sky frame subtraction—simply subtracting a second "object" image from the image under consideration and then flattening the resulting difference image. An example of such a difference image is shown in Fig. 6, from 11 July, which shows Epimetheus nearing the eastern edge of the gap in scattered light from the rings, as well as Enceladus ~4.7″ to the north. In this case, the two 240-sec exposures were taken immediately following one another, but the (earlier) subtracted frame was out of focus. Even though both Epimetheus and Enceladus appear at nearly identical pixel locations in both images, the light is more concentrated in the properly focused image and the moons do not cancel out in the subtraction process. The Enceladus image clearly shows a negative "halo" due to the subtracted out-of-focus frame. The much smoother scattered-light distribution from the rings is indeed substantially reduced by the subtraction process, although imperfect registration of the rings between the two frames results in bright and dark fringes around the edges of the rings. (The rings themselves were saturated in the raw frames and appear neutral gray in Fig. 6.)

Because the offset guider was programmed to keep the target satellite at a constant pixel location from frame to frame (see Section 2.2), this simple subtraction procedure suffers from two generally contradictory constraints: (1) the satellite(s) of interest must appear in one image and not the other so as to avoid cancellation; and (2) the images must be separated by less than ~4 min in time, corresponding to 0.6″ of satellite motion, or the motion of the rings relative to the pixel grid will result in unsatisfactory subtraction of the scattered light. These limitations prevented us from using this method in all but a few cases.

An alternative procedure to image subtraction would be to construct a model of the scattered light distribution and subtract this from the sky-subtracted images such as

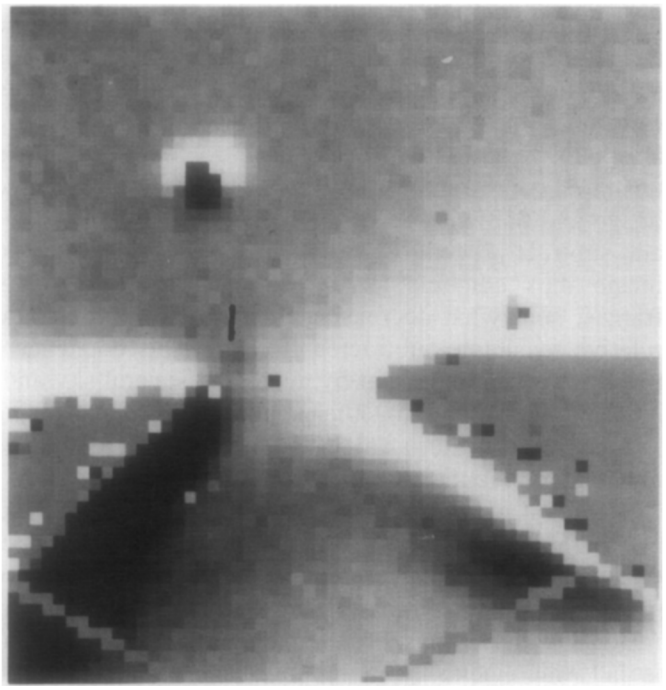

FIG. 6. An IR image of Epimetheus obtained on 11 July 1990 at λ2.30 μm (image 10). North is up, east to the left. A similar out-of-focus image taken at the *same* telescope position immediately beforehand was used for sky subtraction, largely canceling the scattered light from the rings. Epimetheus is indicated by a vertical tick mark, near the left edge of the gap in scattered light from the rings and ~4.7″ south of the much brighter Enceladus. The latter is surrounded by a white halo due to the out-of-focus subtracted image. Grey areas within the rings were saturated in both raw images. Note the excellent seeing, as indicated by the small size (~2 pixels FWHM) of the in-focus satellite images.

Fig. 5. This procedure is commonly used when dealing with the scattered-light profiles from bright stars in crowded fields or in removing the radial gradient in brightness due to a cometary coma in order to reveal faint detail in the tail. However, in these cases the scattered-light distribution is axially symmetric, and a model may be generated either from the point-spread function of the image or by rotationally averaging the measured scattered-light profile of the coma. In the present situation, however, the partial obscuration of the bright rings by the (dark) planet results in a complex scattered-light distribution which does not readily lend itself to simple geometric modeling. Experiments with fitting empirical two-dimensional polynomial functions to similar CCD images of Saturn's rings led to generally unsatisfactory results, because of very steep gradients in the region of the inner satellites (A. Skrutskie 1990, private communication).

A satisfactory solution to the scattered-light problem, which avoids the difficulties both of simple image subtraction and of two-dimensional modeling, is to use either an earlier or later reference image in which the satellite(s) do not appear to subtract the scattered light in the images of interest. In general, this procedure involves first shifting the reference image relative to the object image to account for the motion of the telescope in the intervening time (recall that the offset guider was set to track the satellites, not Saturn). Pixel-to-pixel electronic bias and sensitivity variations across the array, however, make it necessary to first subtract an unshifted sky frame from each object and reference image and flat-field the result before applying this shift-and-subtract procedure. The resulting doubly subtracted image thus combine sky noise from four individual frames, somewhat decreasing their signal-to-noise ratio relative to simple subtracted frames. (This could have been mitigated somewhat by averaging several sky and/or reference frames together, but at the price of using frames taken further away in time from the object image and under potentially different seeing conditions.)

After first resetting all saturated and known "bad" pixels to zero, we determined the optimal spatial shift between the object and reference images by performing a grid of shift-and-subtract tests and computing the rms residual signal in the subtracted images. The optimal shift is that which yields the minimum rms residual. The satellites are too faint relative to the ring light to appreciably influence the residual flux, so this procedure effectively aligns the rings in the two images. Figures 7a and 7b show images of Janus and Epimetheus obtained on 4 July and 14 August, respectively, after the application of this shift-and-subtract procedure. The image shown in Fig. 7a is the same as that shown in Fig. 5, after subtraction of a reference image taken 14.5 min earlier. In addition to the now more clearly resolved image of Janus, Fig. 7a shows

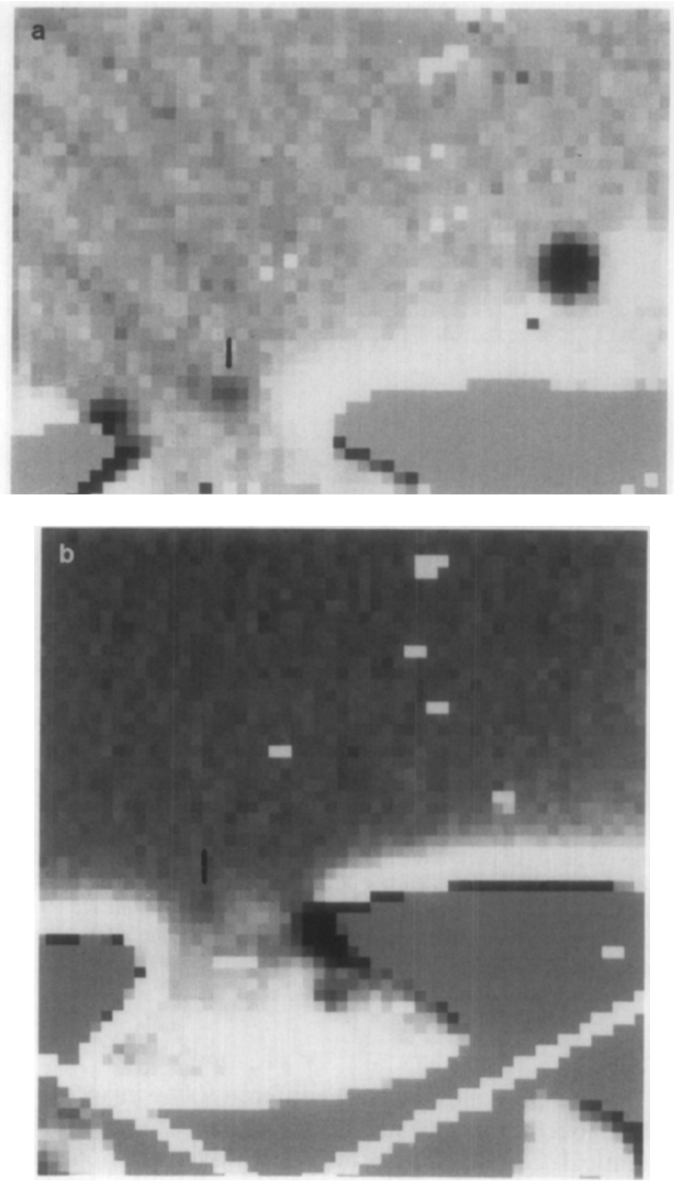

FIG. 7. (a) The image of Janus shown in Fig. 5, after subtraction of a previous image (No. 637) shifted to best align the position of the rings in the two frames. Note the substantial reduction in scattered light in comparison with Fig. 5, with the result that Janus, indicated by the tick mark, is now clearly visible and Mimas has emerged from the halo of scattered light from the rings. The second, white image of Mimas near the right edge of the frame is from the subtracted reference image, taken 14.5 min earlier. Saturated regions on the rings were set to zero and appear a uniform grey. Faint diagonal stripes visible on the sky are due to coherent interference arising in the camera electronics. (b) The best image of Epimetheus obtained on 14 August 1990 (No. 1033), after subtraction of a previous image (No. 1026) shifted to best align the position of the rings in the two frames. North is up, east to the left. The camera field of view is illustrated in Fig. 4b. Epimetheus actually appears twice in this frame: as a black (positive) image displaced 4–5 pixels to the left of a white (negative) image from the subtracted frame, the separation being due to orbital motion during the intervening interval of 9.0 min. Uniform grey areas on both the rings and the planet were saturated in the raw frames and have been set to zero.

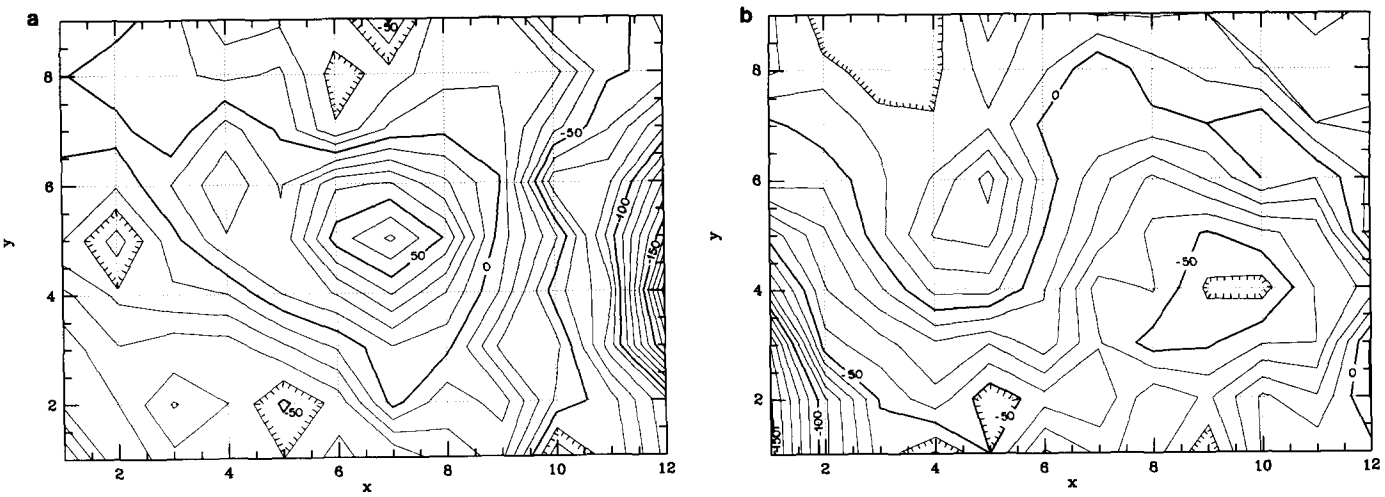

FIG. 8. (a) Contour plot of a 12 × 9 pixel section of the shift-and-subtract image in Fig. 7a, centered on the measured position of Janus at pixel (7,5). Contour interval is 10 DN (data number), where 1 DN corresponds to ~90 electrons in the original image. The array read noise is 5 DN per pixel, and the subtracted sky background was ~4000 DN per pixel, resulting in a 1σ noise level in the raw frames of 8.3 DN. The peak signal from Janus is 72 DN, or 4.3σ in this doubly subtracted frame. Note that, while residual scattered light from the rings is apparent at the right edge of the plot, the satellite image is superposed on a relatively flat local background. (b) Contour plot of a 12 × 9 pixel section of the shift-and-subtract image in Fig. 7b, centered near the measured position of Epimetheus at pixel (5,5). A second, negative image of Epimetheus from the reference frame is seen at pixel (9,4). Contour interval is 10 DN (data number), as in Fig. 8a. The peak positive signal from Epimetheus is 44 DN, or 2.6σ in this doubly subtracted frame. Residual scattered light from the rings is strongest at the lower left corner of the plot, but the positive satellite image is again superimposed on a relatively flat local background.

two images of Mimas: the positive image in Fig. 5 and a negative image displaced ~6 pixels to the right (west) from the earlier reference image.

Figure 7b shows one of the best images of Epimetheus, after subtraction of a reference frame taken only 9.0 min earlier. In this case, both positive and negative images of the smaller coorbital are visible within the gap in scattered light from the rings, due to the relatively short interval between the two frames. Note that, unlike the 2.30-μm image in Fig. 7a which was taken deep in the planetary methane band, the broadband K image in Fig. 7b shows substantial residual flux from the disk of Saturn, in the form of zonal banding and a bright spot near the northwestern limb. In fact, the equatorial regions of the planet are saturated in these images.

Bright and dark fringes visible along the ring edges in Figs. 7a and 7b indicate that the ring alignment is imperfect, although the scattered light is greatly reduced and the visibility of the satellites much enhanced over the original unsubtracted images. Figures 8a and 8b present contour maps of 12 × 9 pixel portions of the images in Figs. 7a and 7b, centered on the coorbital satellites. Both the positive and negative images of Epimetheus are seen in Fig. 8b. From these plots it is apparent that, while regions of residual scattered light extend to within ~5 pixels of the satellite images, the latter no longer are superimposed on strong background gradients which might bias estimates of their positions. Potential refinements to our adopted technique would involve subpixel shifts, necessitating repixellation of the original images to a finer grid spacing, but this was found to be unnecessary for our purposes of satellite detection and position determination. We also preferred to avoid unnecessary resampling of the images. Useful photometric results, however, would certainly require this additional step and have not been attempted for this analysis.

Using the shift-and-subtract technique, we were able to detect Janus in 7 frames on 4 July, and Epimetheus in a total of 21 frames on 4 July and 14 August. In only a few of these cases was the fainter Epimetheus clearly seen in standard sky-subtracted frames. In Fig. 9 we present a time sequence of our best Janus frames from 4 July, in which the orbital motion of both Janus and Mimas is clearly visible. The images in Fig. 9 (frames 642–646) span a total period of 11.6 min, with an average gap of 1.2 min between successive 2-min exposures. The same reference image (No. 637) was used for all four frames. Both positive and negative images of Mimas are visible in each frame, as well as a single positive image of Janus. (Pairs of white pixels represent bad elements in the array, displaced by the shift-and-subtract procedure. They provide a convenient indicator of the shift vector.) This set of images, in which the satellite is cleanly separated from the rings and is also observed to move as predicted (see Fig. 10), provides the most compelling evidence that we have indeed successfully detected the coorbital satellites.

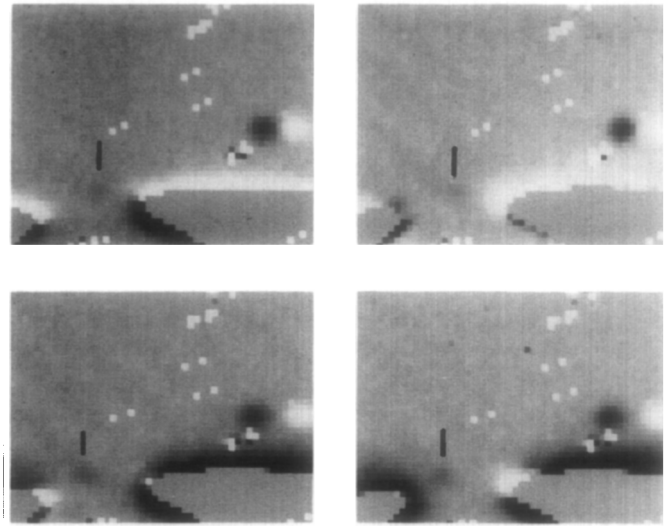

FIG. 9. A time series of Janus images obtained on 4 July 1990, showing the motion of the satellite from right to left (west to east) across the gap in scattered light from the rings. The camera field of view is illustrated in Fig. 4a. Frames 642, 643, 645, and 646 are shown, with time increasing from top left to bottom right. Individual images were shift-and-subtracted as in Fig. 7, using a common reference image (No. 637), which produced both black (positive) and white (negative) images of Mimas in each frame. Pairs of "bad" pixels indicate the magnitude and direction of the frame shift.

3.2. *Astrometry*

For each frame showing a clearly discernable image of either Janus or Epimetheus, the pixel coordinates of the coorbital satellite plus that of the reference satellite, if available, were determined. For the numerous 4 July and 14 August data we used images obtained from the shift-and-subtract procedure, as described above and illustrated in Figs. 7 and 9. For the two 11 July images of Epimetheus, subtracted images such as that in Fig. 6 were used. For the single Janus image of 1 July and the three Epimetheus images of 13 July we measured standard sky-subtracted images, and these measurements are given correspondingly lower weights in the orbital fits. Wherever possible, it is obviously desirable to determine the centroid of an image in order to estimate its position to subpixel accuracy. Centroid measurements of the faint Jovian satellites Metis and Adrastea, obtained from frames taken with the same IR camera, yielded postfit rms residuals of 0.15″–0.20″, or $\frac{1}{2}$ to $\frac{2}{3}$ of a pixel (Nicholson and Matthews 1991). For the images of the larger satellites, Enceladus, Tethys, and Rhea obtained on 14 August, we derived centroid positions by fitting and subtracting the local background in an annulus around the object and then computing the center-of-light of the residual flux within a small aperture centered on the satellite.

This standard centroiding procedure proved impractical, however, both for the images of Janus and Epimetheus nestled within the narrow gap in the scattered light from the rings and for Mimas due to its close proximity to the rings in most frames. In order for a successful centroid determination, it is generally necessary to define both an inner circular measurement aperture of radius at least 2–3 pixels, and an outer annular aperture of radius at least 3–5 pixels within which the local sky background is determined. Inspection of Figs. 8a and 8b shows that, with the satellite approximately centered in the "gap," even a 3-pixel radius sky annulus would be potentially contaminated by residual scattered light from the nearer ring edge. Any such contamination by this scattered light, with its strongly nonuniform gradient, would be likely to severely bias the derived centroid, as we confirmed in several attempts to make this technique work satisfactorily. On the other hand, the background light gradients at the locations of the satellite images themselves were generally small, as may be seen in Fig. 8, permitting a fairly unbiased eyeball estimate of the satellite's location.

We therefore chose, after experimentation with several centroiding routines, to rely on visual estimates for the centers of all coorbital satellite and Mimas images. We estimated the a priori uncertainties of positions derived from subtracted images at ±(0.5–1) pixel, or 0.15″–0.3″, depending on the scattered light geometry in each image. In order to reduce subjective biases as much as possible, all measurements were made independently by two people, generally at several different contrast enhancements of the image, and in some cases using different reference images; the variations were consistent with the assigned uncertainties. These estimated errors are also consistent with the post-fit residuals from our orbital fit, as shown in Figs. 13 and 14 below. Typical FWHM satellite image diameters are ~1″ (cf. Fig. 8), and because of the guider update procedure adopted for the longer (>120-sec) exposures, no appreciable orbital smear is detectable in the images.

3.2.1. Satellite–satellite astrometry. For the observations on 1, 4, and 11 July, images of either Mimas or Enceladus are available in each frame and permit straightforward satellite–satellite relative measurements. In terms of the measured pixel coordinates of target and reference satellites, (x, y) and (x_R, y_R), and the known camera scale, $S = 0.313''$ per pixel (Nicholson and Matthews 1991), the relative position of Janus or Epimetheus is given by:

$$\Delta\alpha_{rel} = -S(x - x_R),$$

$$\Delta\delta_{rel} = S(y - y_R).$$

The orientation of the pixel grid in the camera relative to north on the sky was determined from previous observations with the identical instrument and telescope mounting

TABLE IIa
Satellite–Satellite Measurements

Date (1990)	Frame #	UTC (hrs)	Satellites*	$\Delta\alpha_{rel}('')$	$\Delta\delta_{rel}('')$
1 July	184	12.3383	Ja Mi	0.00	- 2.66
4 July	640	6.9958	Ja Mi	8.92	- 3.13
	641	7.0328	Ja Mi	8.76	- 3.13
	642	7.0708	Ja Mi	8.92	- 2.97
	643	7.1103	Ja Mi	8.76	- 3.45
	645	7.1933	Ja Mi	9.08	- 3.45
	646	7.2314	Ja Mi	8.92	- 3.29
	647	7.2689	Ja Mi	9.08	- 3.13
4 July	673	8.7797	Ep Mi	- 4.70	- 1.56
	674	8.8686	Ep Mi	- 4.70	- 1.56
	675	8.9728	Ep Mi	- 4.69	- 1.57
	676	9.0444	Ep Mi	- 4.70	- 1.57
11 July	10	7.8111	Ep En	- 0.94	- 4.69
	11	7.8889	Ep En	- 0.62	- 4.70

* Coorbital satellite: Ja, Janus; Ep, Epimetheus. Reference satellite: Mi, Mimas; En, Enceladus.

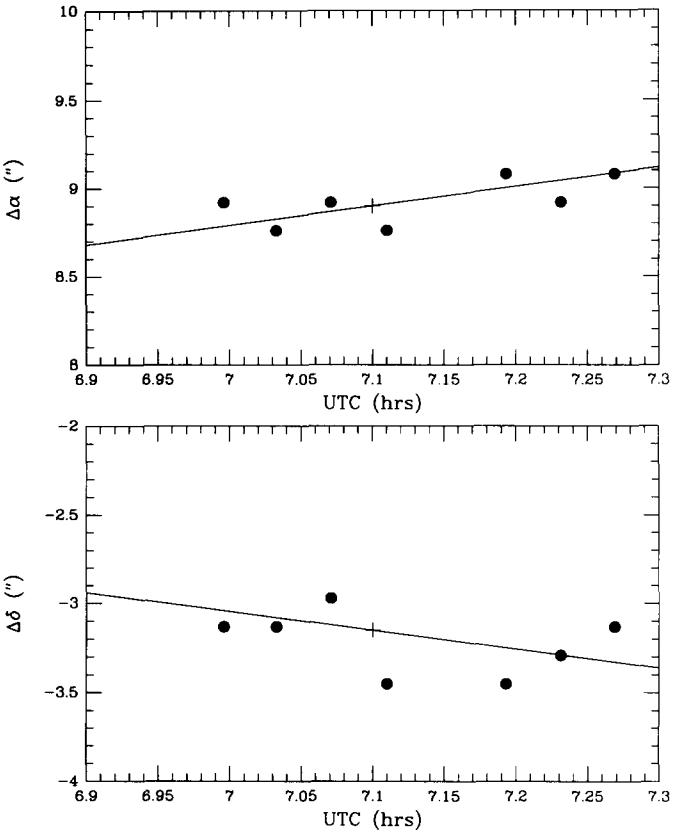

FIG. 10. Differential positions of Janus relative to Mimas from seven images on 4 July 1990, as a function of midexposure time (see Table IIa). Straight lines with slopes calculated from the satellite ephemerides have been adjusted vertically to give the best fit to the observations. Crosses indicate the normal point used in the orbit fit.

plate (Nicholson and Matthews 1991, Table I), from a combination of observed planetary and satellite motions and the orientation of diffraction spikes due to the spider supporting the secondary mirror. The measured rotational offset of 2.6° ± 0.3° relative to apparent north was corrected for in the present observations by rotating the telescope baseplate by 2.5°, and running north–south and east–west tests with the chopping secondary. No additional rotational correction to the measured separations is thus required.

The resulting offsets, in mean equatorial coordinates of date, are given in Table IIa with the corresponding frame numbers and midexposure observation times. These individual relative positions are estimated to be accurate to ±1 pixel, or ±0.3". The 4 July data for Janus and Epimetheus are plotted in Fig. 10 and Fig. 11, respectively, fitted by straight lines with slopes predicted by the satellite ephemerides, but adjusted vertically to best fit the observations. At conjunction, the velocities of the coorbitals relative to Mimas or Enceladus are quite low: ~1.0"/hour in right ascension (RA) relative to Mimas and ~1.7"/hour relative to Enceladus, as compared with rates of ~9"/hour in RA relative to Saturn. In consequence, the average relative positions are quite well determined from multiple images. Typically, only 1–2 pixels of relative motion were detected over the 15–20 min of continuous observation possible on each orbit.

TABLE IIb
Planetocentric Measurements

Date (1990)	Frame #	UTC (hrs)	Satellite*	$\Delta\alpha$ (")	$\Delta\delta$ (")
14 August	1020	8.6600	Ep	0.87	9.01
	1021	8.6792	Ep	1.14	9.04
	1022	8.6983	Ep	1.42	9.37
	1023	8.7175	Ep	1.07	9.39
	1024	8.7367	Ep	1.34	9.10
	1025	8.7561	Ep	1.31	8.81
	1026	8.7753	Ep	1.89	9.15
	1027	8.7944	Ep	2.17	9.48
	1028	8.8136	Ep	2.13	9.51
	1030	8.8669	Ep	2.96	8.94
	1031	8.8861	Ep	2.93	9.28
	1032	8.9053	Ep	2.89	8.99
	1033	8.9247	Ep	2.85	9.01
	1034	8.9439	Ep	3.13	9.03
	1035	8.9631	Ep	3.09	9.06
	1036	8.9822	Ep	3.05	9.08
	1037	9.0014	Ep	3.01	9.10

* Ep, Epimetheus.

3.2.2. Planet–satellite astrometry. On 14 August, no suitable reference satellite was present within the field of view of the IR camera. We therefore, as described in Section 2.2.4 above, obtained images of Mimas, Enceladus, Tethys, and Rhea at known offset-guider positions

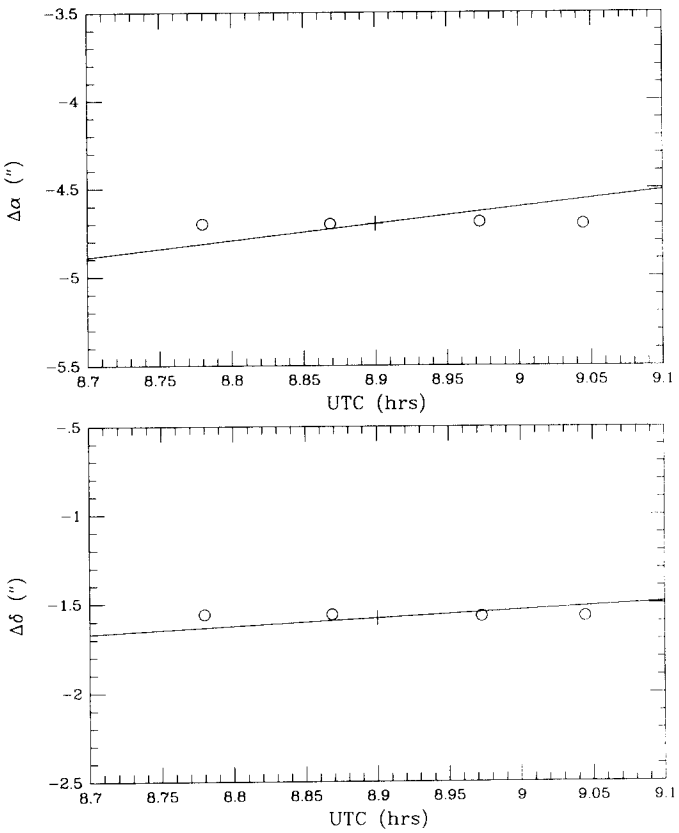

FIG. 11. Differential positions of Epimetheus relative to Mimas from four images on 4 July 1990, as a function of midexposure time (see Table IIa). Straight lines with slopes calculated from the satellite ephemerides have been adjusted vertically to give the best fit to the observations. Crosses indicate the normal point used in the orbit fit.

immediately following the observations of Epimetheus. The guider was set to track Titan continuously during the period of observations. The planetocentric position of the target object, located at pixel position (x, y), is given in terms of the guider's offset setting $(\Delta\alpha_G, \Delta\delta_G)$ and the calculated planetocentric position of Titan $(\Delta\alpha_T, \Delta\delta_T)$ by

$$\Delta\alpha = \Delta\alpha_T - \Delta\alpha_G - S(x - x_0),$$
$$\Delta\delta = \Delta\delta_T - \Delta\delta_G + S(y - y_0),$$

where (x_0, y_0) is the (initially unknown) array position corresponding to the zero point of the offset guider. By fitting the derived positions of Enceladus, Tethys, and Rhea to those given in the 1990 Astronomical Almanac, we determined that $x_0 = 27.5, y_0 = 32.9$. The rms residuals for a total of seven observations of these three satellites were 0.08" in each coordinate, or ~0.3 pixels. (In addition to fitting the zero point, we also checked the scale and rotational zero for the guider offset, finding small corrections of 0.7% in the nominal scale and 0.10° in the nominal position angle settings.)

The resulting planetocentric positions of Epimetheus on 14 August, estimated to be accurate to ±1 pixel, or ±0.3", are given in Table IIb and plotted in Fig. 12. As in Figs. 10 and 11, the straight lines fitted to the data have slopes given by the satellite ephemeris and only the vertical positions of the lines have been adjusted. In this case, the rapid orbital motion of the satellite in RA is readily apparent, and is consistent—within ±1 pixel—with the predicted motion. We note here that the data in Fig. 12 provide a test of possible systematic biases in our visual-position measurements due to background light gradients: at ~8:40 hrs (UTC) and at ~9:00 hr, Epimetheus was located close to the western and eastern edges of the gap in scattered light from the rings (cf. Fig. 4b), where the scattered light is most severe, but with oppositely directed east–west gradients. An up-gradient bias, which might be expected, would displace the satellite images in such a

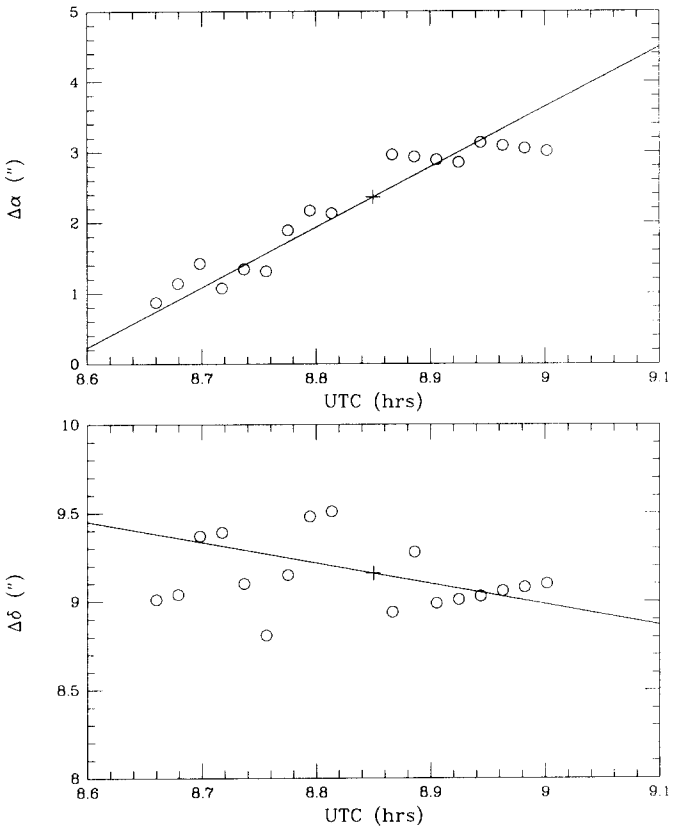

FIG. 12. Planetocentric positions of Epimetheus derived from 17 images on 14 August 1990, as a function of midexposure time (see Table IIb). Straight lines with slopes calculated from Epimetheus' ephemeris have been adjusted vertically to give the best fit to the observations. Note that, aside from the ±0.3" (1 pixel) scatter in individual frames, the rate of orbital motion is in good agreement with the prediction. Crosses indicate the normal point used in the orbit fit.

way as to increase the apparent orbital motion over the true value. No evidence for such an anomalous motion in RA (≈orbital longitude) is seen in Fig. 12, where the measured points fit well the predicted slope. (A test of possible systematic error in declination is provided below.)

3.2.3. Satellite–ring astrometry. As noted above, on 13 July no nearby reference satellites were available, and no offset observations were made as on 14 August. Unfortunately, it did not prove possible to transfer the guider zero point with confidence from 14 August to 13 July, as the instrument had been dismounted from the telescope in the interim. As a last resort, we used the three available images to estimate crudely the time at which Epimetheus passed superior conjunction, by reference to the "cusps" of the rings where they were cut off by the planet and its shadow. The estimated time of conjunction, 9:41 ± 3 min UT, is 2 min ahead of the prediction. From the known longitude of superior conjunction, this time was converted directly to an approximate orbital longitude on this date for input to our orbit model (see Table IV below).

3.3. Normal Positions

For input to the satellite dynamical model, we have chosen to use normal points for each satellite on each night of observation. The motivation for this procedure, as opposed to directly fitting each measured position individually, is as follows. First, the individual measurements are estimated to be uncertain by ±1 pixel, or ±0.3″, whereas the average of several (4–17) measurements is likely to be rather better than this, except for systematic errors. Second, the IR data are used below only to refine the parameters of the 8-year librational motion, and not the elliptical orbital elements which are much better determined by the Voyager observations (Yoder *et al.* 1989), so we are not interested in fitting the motion within a single night's observations. Third, the individual measurements from previous observations in 1966, 1980, and 1981 have likewise been converted by Yoder *et al.* (1989) to single measurements of longitude at convenient reference times (see Table IV) for input to the orbit model. Using the full set of IR measurements, without the corresponding full sets of spacecraft measurements and previous Earth-based data, would unduly weight the present data in the fits.

From the fits to the 4 July satellite–satellite data in Figs. 10 and 11, we derive the normal points given in Table III, relative to Mimas. On 1 July, only a single measurement of Janus is available, again relative to Mimas. For 11 July, we adopt the average of the two measurements relative to Enceladus and assign this to the mid-time between the two exposures. For 14 August, the fits in Fig. 12 were used to derive a normal planetocentric position for Epimetheus. The estimated time of conjunction for Epimetheus on 13 July was directly converted to a mean longitude (see above) and thus does not appear in Table III. The adopted uncertainties in these normal positions, reflecting the fit uncertainties, are discussed below.

TABLE III
Normal Points Derived from the 1990 Palomar IR Data

Date (1990)	UTC (hr)	Satellites		Relative position $\Delta\alpha_{rel}$	Relative position $\Delta\delta_{rel}$	Ref. satellite* $\Delta\alpha_R$	Ref. satellite* $\Delta\delta_R$	Derived position $\Delta\alpha$	Derived position $\Delta\delta$
1 July	12.338	Ja	Mi	0.00	−2.66	−0.04	11.82	−0.04	9.16
4 July	7.100	Ja	Mi	8.90	−3.15	−8.32	12.35	0.58	9.20
4 July	8.900	Ep	Mi	−4.70	−1.58	5.55	10.93	0.85	9.35
11 July	7.850	Ep	En	−0.78	−4.70	3.60	14.01	2.82	9.31
14 Aug.	8.850	Ep		—	—	—	—	2.36	9.16

[a] Ephemeris from D. Taylor (1990, private communication).

3.3.1. Reference satellite ephemerides. Planetocentric normal positions, $\Delta\alpha$ and $\Delta\delta$, were derived from the satellite–satellite positions of 1, 4, and 11 July in Table III using ephemerides for Mimas and Enceladus calculated by D. B. Taylor of the Royal Greenwich Observatory (1990, private communication) based on a refined version of the orbital solution of Taylor and Shen (1988). In Table III we give the interpolated Mimas or Enceladus position and the resulting planetocentric coorbital satellite positions used in our revised orbital solution below.

We note here that preliminary reductions of our 4 July data, using Mimas ephemerides from either the 1990 Astronomical Almanac or the Jet Propulsion Laboratory ephemeris files (Jacobson 1990, private communication) resulted in substantial residuals for both Janus and Epimetheus relative to the orbital model of Yoder *et al.* (1989). These residuals were clearly incompatible with much smaller residuals obtained for Epimetheus on 11 July and 14 August, when other satellites were used as a reference objects (Nicholson *et al.* 1990). On 4 July our observed locations for both Janus and Epimetheus (referred to the JPL Mimas ephemeris) fell 1.7°–2.0° ahead of the model of Yoder *et al.* (1989), whereas those of Epimetheus on 11 July and 14 August (referred to Enceladus, and to a composite of Enceladus, Tethys, and Rhea, respectively) fell within 0.2°–0.4° of the same model.[3]

Interpreted as errors in Mimas' position rather than in the coorbital ephemerides, the 4 July data imply a Mimas longitude residual of −1.5° ± 0.5° relative to the JPL ephemeris. A similar apparent Mimas residual of −2.2°

[3] At conjunction in 1990, 1.0° in longitude for Janus or Epimetheus, representing 2.78 min of orbital motion, corresponded to 2640 km or 0.404″. The corresponding numbers for Mimas are 1.0° = 3.77 min = 3240 km = 0.495″.

$\pm$ 0.8° was noted for 1 July, though these data are much poorer. Finally, our own direct measurement of Mimas' position on 14 August relative to Enceladus, Tethys, and Rhea also yielded a longitude residual of $-1.5° \pm 0.7°$ relative to the JPL ephemeris. All of this evidence points to a longitude error in the JPL Mimas ephemeris of $\sim 1.5°$, in the sense that the satellite was behind its predicted position in July/August 1990. Jacobson (1991, private communication) has confirmed that the current JPL ephemeris files for the Saturnian satellites reflect only fits to pre-Voyager Earth-based observations and have not been updated to include Voyager optical navigation data.

It might be inquired as to whether this apparent longitude error is due to some systematic error in the measurements. In the case of the 1 and 4 July observations, both the coorbital satellite and Mimas were measured on the same frame, so differential refraction or wavelength-dependent effects are unimportant. (We assume that all three satellites have similar icy spectra, as suggested by their high visual albedos.) The 14 August measurements combined data from different frames, all at the same wavelength of 2.2 μm, but employed the offset guider which operates in the visual for the astrometric linkage of the frames. We have confirmed that the appropriate differential refraction correction for 2.2 μm was indeed programmed into the guider, so that changes in differential refraction with airmass were correctly accounted for. We also note that the apparent errors in Mimas' longitude are independent of the position of Mimas relative to Saturn.

Taylor's ephemeris, used for all the astrometric results presented in this paper, differs from the JPL ephemeris at the time of our observations by an average of $-0.78°$ in longitude for Mimas, but by only $+0.10°$ for Enceladus. Although the Mimas correction is somewhat less than that inferred above, it is in the same direction and we find no significant systematic residuals that exceed the estimated uncertainties in any of our measurements when the Taylor ephemerides are used for Mimas and Enceladus. It is therefore unclear from our data whether or not there remains an error of order $+0.7°$ in longitude in the Taylor ephemeris.

3.3.2. Astrometric uncertainties. The normal positions in Table III, together with the weaker 13 July observation, constitute the input from the Palomar IR observations to the revised orbital solution in Section 4. The uncertainties assigned to these normal positions depend on the number of individual measurements combined in each point, uncertainties in these measurements, and systematic errors in the reference satellite ephemerides. For the 4 July and 14 August observations, which are the most numerous, we assign uncertainties of $\pm 0.15''$, corresponding to $\pm 0.37°$ in longitude. (Although the formal precision of the 14 August normal point is better than this, we consider it unlikely, given the discussion in Section 3.3.1 above, that the reference satellite ephemerides are accurate to better than $\pm 0.1''$.) The more limited data from 1 July and 11 July lead to assigned uncertainties of $\pm 0.35''$, or $\pm 0.87°$, for these dates. For 13 July, with no reference satellite observations, the estimated error in the time of superior conjunction of ± 3 min yields a longitude uncertainty of $\pm 1.2°$.

4. REVISED ORBITAL SOLUTION

4.1. Theoretical Background

We find that simple analytic models can be used to fit both the available Voyager spacecraft data and ground-based telescopic observations of the coorbital satellites to within their uncertainties. The orbits are represented as inclined, precessing ellipses with eccentricities and inclinations fixed at values determined by the Voyager imaging data (Yoder *et al.* 1989). The apsidal rate $\dot{\varpi}$ and nodal rate $\dot{\Omega}$ are calculated using the known Saturnian gravity field coefficients (Null *et al.* 1981, Nicholson and Porco 1988), the classical satellites' known masses, and the Sun's action. The slow change in relative mean longitude $\phi = \lambda_1 - \lambda_2$ (1 denotes Janus and 2, Epimetheus) caused by their mutual interaction is modeled using a constant Hamiltonian, H (Yoder *et al.*, 1989),

$$H = \dot{\phi}^2 + 3\frac{M_t}{M_S}\frac{n_0^2}{x}K\left\{1 + 4x^3 + \frac{f(e, I, \phi)}{x^2}\right\},$$

where $M_t = M_1 + M_2$ is the sum of the satellite masses, M_S is Saturn's mass, n_0 is the average mass-weighted mean motion, and

$$x = |\sin(\phi/2)|,$$
$$K = (1 + \tfrac{3}{2}J_2(R_S/a)^2).$$

The function $f(e, I, \phi)$ is of order e^2 or I^2 (see Yoder *et al.* for the explicit expression).

The mean longitude λ for each satellite is given by

$$\lambda_i = \beta_i\phi + n_0(t - t_0) + \theta,$$

where t_0 is a reference epoch (24.0 Aug 1981) fixed near the Voyager 2 encounter and θ is a phase constant. The mass fraction parameter β_1 is

$$\beta_1 = \frac{M_2}{M_1 + M_2},$$

while $\beta_2 = \beta_1 - 1$ (note that β_2 is negative). We solve for

just one, β_1, which hereafter is designated as β. There are six adjustable constants in this model: H, M_t, β, n_0, θ, and ϕ (t_0).

The very accurate Voyager flyby data effectively fix the Keplerian constants e_i, I_i, θ, and $\phi(t_0)$, but only weakly constrain the remaining constants because of the short time span (286 days) separating the two flybys, compared to the 2927-day libration period, and because no satellite close approach occurred during 1980/1981.

On 31 August 1979, approximately $1\frac{1}{2}$ years prior to the Voyager 1 flyby, a single Pioneer 11 image of Epimetheus was obtained (Van Allen 1982). During February–April 1980, groundbased observations of both objects were acquired as the Earth passed through Saturn's ring plane. These data are 1 to 2 orders of magnitude less accurate than Voyager data as a whole and are also too close in time to be particularly useful as independent measurements, but are included in our fit as a further check on the model and to provide an additional test of the accuracy of groundbased observations.

The discovery data obtained during the 1966 ring-plane crossing are sufficiently distant in time for the accumulated effect of several close encounters to have significantly altered the satellite longitudes relative to those predicted for purely Keplerian orbits. Because Janus' position was well determined at this epoch, and Janus and Epimetheus were then separating instead of closing as occurred in 1979–1981 (see Fig. 2), the mass fraction β and mean motion n_0 are well constrained by Janus' measured position at this epoch. Unfortunately, the remaining parameters H and M_t, which contain the most interesting information, require an accurate (and sure) detection of Epimetheus. As discussed in Section 1, the proposed detection of Epimetheus in December 1966 failed this criterion because of an apparent near overlap of Prometheus and Epimetheus in the sequence of images obtained by R. L. Walker (Yoder *et al.* 1989). The Palomar observations were specifically targeted at Epimetheus in order to tie down the remaining model constants with certainty.

4.2. The Revised Solution

The first step was to convert the Palomar IR normal points listed in Table III from planetocentric positions to mean longitude at each epoch of observation. The effects of orbital eccentricity and inclination were removed using the Voyager 1 and 2 joint solution (see Table VI in Yoder *et al.* 1989) and the calculated apsidal and nodal rates $\dot{\varpi}$ and $\dot{\Omega}$. The resulting data are listed in Table IV, together with the data analyzed in the earlier paper.[4] Note that the epochs of observation have also been converted to Barycentric Dynamical Time (TDB) and corrected for light travel time from Saturn. The adopted value for ΔTT = TDB − UTC was 57.184 sec.

TABLE IV
Data Used in Orbit Model Solutions

Satellite*	Mean Longitude (deg)	Mean Motion (deg/day)	Julian Date (TDB at Saturn)
	18 Dec. 1966 – Ring Plane Crossing		
1	374.55 ± 0.36		2439477.5
2	287.80 ± 2.00		2439477.5
	31 Aug. 1979 – Pioneer 11 Flyby		
2	239.6 ± 2.0		2444117.45250
	22 March 1980 – Ring Plane Crossing		
1	198.38 ± 0.30		2444320.5
2	33.21 ± 2.00		2444320.5
	29 Oct. 1980 – Voyager 1 Flyby		
1	248.9305 ± 0.0346	518.2437 ± 0.0050	2444541.5
2	138.8832 ± 0.0381	518.4894 ± 0.0033	2444541.5
	24 Aug. 1981 – Voyager 2 Flyby		
1	41.7593 ± 0.0381	518.2342 ± 0.0047	2444840.5
2	7.3870 ± 0.0296	518.4931 ± 0.0035	2444840.5
	1 July - 14 Aug. 1990 – Palomar IR		
1	120.25 ± 0.87		2448073.96276
1	121.59 ± 0.37		2448076.74449
2	121.22 ± 0.37		2448076.81949
2	125.29 ± 0.87		2448083.77582
2	120.82 ± 1.24		2448085.85153
2	121.30 ± 0.37		2448117.81673

* 1, Janus; 2, Epimetheus.

The solution for the total mass and the other five parameters is listed in Table V. Instead of H, we have solved for the mean libration rate $\dot{\phi}(60°)$ at the leading Langrangian point (i.e., the point where Epimetheus trails Janus by 60°), partly because a smaller correlation of parameters is achieved for this choice, and partly because this rate has a physical meaning, namely the maximum rate of angular separation or approach (Yoder *et al.* 1983). A corrected version of solution 3 from Yoder *et al.*'s (1989) Table VIII is also listed for comparison. We find excellent agreement between these two solutions, but with significantly improved values for n_0 and M_t when the 1990 observations are included. An

[4] The original solutions for mean longitudes for the 1966 and 1980 groundbased data have been slightly altered here (by less than 1σ) because of computer model errors discovered while fitting the Palomar IR observations.

TABLE V
Model Solution Parameters

Solution	M_t (10^{21} g)	$\dot{\phi}(60°)$ (deg/day)	n_0 (deg/day)	β	ϕ_0 (deg)	θ (deg)
1	2.53	0.25500	518.29170	0.21665	34.426	34.323
σ	± 0.15	± 0.00028	± 0.00005	± 0.00049	± 0.028	± 0.029
2	2.62	0.25507	518.29172	0.21670	34.428	34.321
σ	± 0.26	± 0.00031	± 0.00010	± 0.00059	± 0.028	± 0.031

Note. Solution 1 includes all available spacecraft and groundbased data. Solution 2 excludes the 1990 Palomar IR data and is essentially identical to solution 3 of Yoder *et al.* (1989). The solution epoch, t_0 = 24.0 August 1981, TDB = JD 244 4840.5.

indication of the reliability of this solution is indicated by the postfit longitude residuals in Fig. 13. The fact that all error bars cross the zero line suggests that (1) there has been no significant omission of additional orbit perturbations, and (2) that the adopted data uncertainties are probably conservative.

The uncertainties assigned to our normal points may be significantly overestimated: the rms residual for the six 1990 points relative to a local fit for mean longitude is only 0.2° (0.07″), compared with the a priori uncertainties of at least 0.37°. However, this could conceal systematic biases in the IR data of order ±0.15″, due either to ephemeris errors in the reference satellites or to image center bias arising from scattered light from the rings (see discussion in Section 3.2 above). The Palomar normal points listed in Table III in terms of right ascension and declination can be rotated so that the y component is aligned with the projection of Saturn's north pole. Since most of the measurements were taken near superior conjunction, the x component alone is sensitive to satellite longitudes. The y component is primarily sensitive to the satellite inclinations and nodes, which are supposedly well constrained by the Voyager data. A test for possible systematic errors can thus be obtained from a comparison of the observed and predicted y offsets, as shown in Fig. 14. A marginally significant mean residual of $\langle \delta y \rangle \simeq 0.11'' \pm 0.08''$ is found, which may result from the north–south gradient in scattered light from the rings. A similar bias might conceivably affect the x measurements, although we have argued in Section 3.2.2 that any systematic east–west error is small and comparable to our adopted uncertainties.

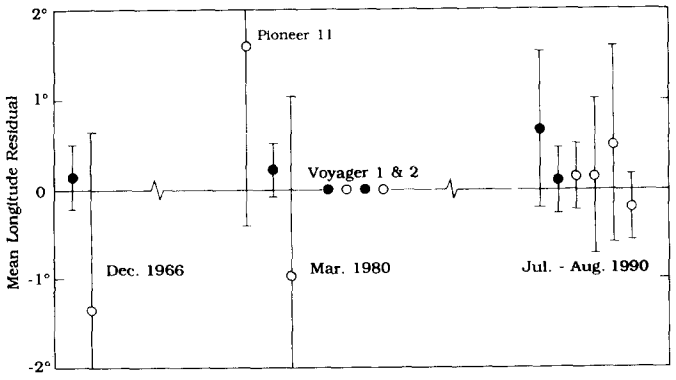

FIG. 13. Longitude residuals for Janus (filled circles) and Epimetheus (open circles) from the best-fitting orbit model (solution 1 in Table V). The fitted longitudes are listed in Table IV. No systematic deviations from the model are apparent, and the a priori error bars may actually be somewhat overestimated for the 1990 data.

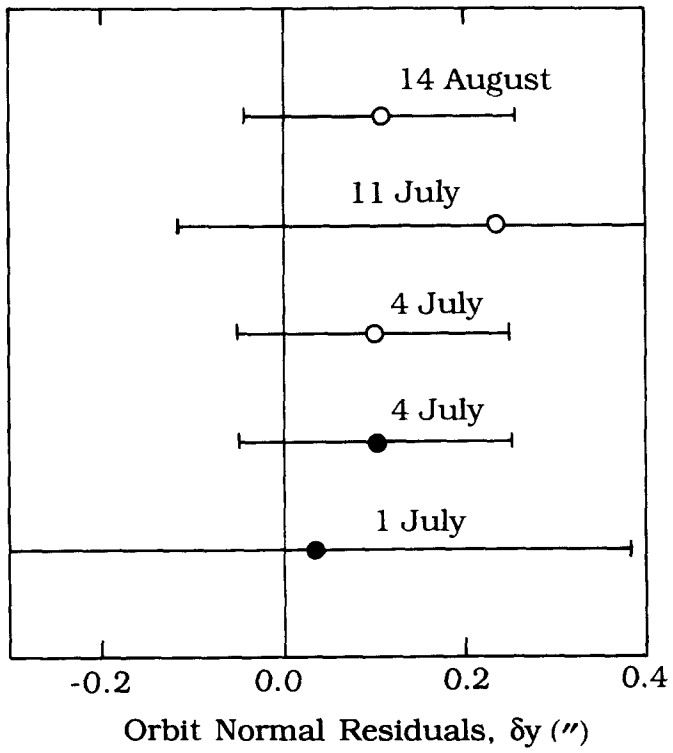

FIG. 14. North–south residuals, δy, of the 1990 Palomar normal points from the best-fitting orbit model. Filled and open circles denote Janus and Epimetheus, respectively. The orbital inclinations and nodes are derived from the Voyager observations and have *not* been adjusted to fit the new data (see text). A systematic residual of ~0.11″ is evident, suggesting a possible small systematic bias in the image positions due to the north–south gradient in scattered light from the rings.

5. DISCUSSION

5.1. Densities and Shapes

The improved values for total mass M_t and mass fraction $\beta = M_2/M_t$ can be used to derive the individual masses. Using solution 1 in Table V, we find

$$M_1 = (1.98 \pm 0.12) \times 10^{21}\ \text{g}$$

$$M_2 = (0.55 \pm 0.03) \times 10^{21}\ \text{g}.$$

The volumes of these satellites are estimated from ellipsoidal fits to their figures to be (Yoder *et al.* 1989, Thomas 1989)

$$V_1 = (3.03 \pm 0.30) \times 10^6\ \text{km}^3$$

$$V_2 = (0.88 \pm 0.14) \times 10^6\ \text{km}^3,$$

from which we may calculate the mean densities

$$\rho_1 = 0.65 \pm 0.08\ \text{g cm}^{-3},$$

$$\rho_2 = 0.63 \pm 0.11\ \text{g cm}^{-3}.$$

Uncertainties in the volumes of these rather irregularly shaped satellites are the major source of error in estimating their densities, although we note that independent estimates of Janus' volume by Thomas (1989) and by Yoder *et al.* (1989) differed by only 3%. Yoder *et al.* (1989) obtained similar densities of $\rho_1 = 0.67 \pm 0.10$ g cm^{-3} and $\rho_2 = 0.64 \pm 0.12$ g cm^{-3}, using data from 1966 and 1979–1981 only, but the current solution is based on a much more robust data set for Epimetheus and is correspondingly more reliable.

These densities are the lowest values yet determined for any icy body in the solar system, excluding comets. Furthermore, Janus and Epimetheus are the smallest bodies—after Phobos and Deimos—for which the mean densities are reliably known. For none of the other 22 small satellites associated with the ring systems of the outer planets (Nicholson and Dones 1991) is there an accurate mass determination. Mimas and Miranda, with mean radii of 200 and 236 km, roughly double that of Janus, have mean densities of 1.14 ± 0.02 and 1.35 ± 0.39 g cm^{-3}, respectively (Dermott and Thomas 1988, Johnson *et al.* 1987). The larger icy satellites of Saturn and Uranus all have mean densities in the range 1.2–1.7 g cm^{-3}.

Further evidence for such unusually low densities for the coorbitals, as well as for the F-ring shepherds Prometheus and Pandora, comes from the analysis of density waves driven in Saturn's rings. Rosen *et al.* (1991) find masses of $1.31^{+1.7}_{-0.3} \times 10^{21}$ g for Janus and $0.33^{+0.11}_{-0.06} \times 10^{21}$ g for Epimetheus, corresponding to densities of $0.45^{+0.65}_{-0.08}$ and $0.49^{+0.23}_{-0.15}$ g cm^{-3}, respectively. (Although it is the smaller satellite, the mass of Epimetheus is actually better determined because its resonances lie interior to those of Janus, resulting in a clean first cycle, while the stronger Janus waves suffer interference from those due to Epimetheus.) They obtain similar densities of $0.27^{+0.16}_{-0.14}$ g cm^{-3} for Prometheus (mean radius 50 km) and $0.42^{+0.28}_{-0.24}$ g cm^{-3} for Pandora (42 km). These results are, of course, somewhat dependent on the applicability of the standard linear-density wave model (Shu 1984), but the consistency between two such completely independent sets of mass estimates is striking.

The simplest interpretation of these low mean densities is that both coorbitals have significant void space within their interiors. The minimum porosity is ~30% for a bulk composition of water ice with a negligible rock fraction, and ~50% for a composition closer to the canonical icy satellite mix of 60% ice and 40% silicates (Johnson *et al.* 1987). Although average porosities of this order are unlikely to be realized in the larger icy satellites, due to gravitational compaction, a substantial porosity for satellites the size of Janus (mean radius 90 km) and Epimetheus (59 km) is in fact consistent with recent models for Mimas. Dermott and Thomas (1988) found the shape of Mimas to be a triaxial ellipsoid in hydrostatic equilibrium, from which they determined a dimensionless polar moment of inertia, C/MR^2, of 0.35 ± 0.01. In combination with the mean density, this implies either that Mimas is differentiated (with a rocky core and icy mantle) or that it is chemically homogeneous but with a substantially underdense outer layer. In the absence of a plausible model for the heating necessary to promote differentiation, the low-density or porous model seems more likely. Such a model for Mimas, consistent with both the mean density and moment of inertia, has been constructed by Eluszkiewicz (1990), using a homogeneous 60–40% ice–rock mixture with a solid density of 1.45 g cm^{-3}. The calculation is based on a physical densification model, driven by hydrostatic pressure and chondritic heat production over a period of 4.5×10^9 years. He finds that the outer ~50 km of Mimas (corresponding to a basal hydrostatic pressure of ~20 bars) may have retained an initial porosity of ~30%, while the central regions have been compressed to solid densities. Perhaps coincidentally, this degree of porosity is exactly that implied by our mean densities for Janus and Epimetheus, for a pure water-ice composition. Since Janus' central pressure is only 4.8 bars, equivalent to that at a depth of 21 km in Mimas' mantle, it seems quite possible that the coorbital satellites, like Mimas, may have formed in a highly porous state, but that their smaller sizes prevented any significant subsequent self-compaction.

Janus' shape is clearly not the result of hydrostatic relaxation in response to internal stresses caused by rotation and the distorting gravitational pull of Saturn. The small static tidal stresses are at most a few bars in the interior, too small to crush or cause plastic flow in ice at the low internal temperature expected in this body. Moreover, the observed shape (principal radii $a = 99.3 \pm 3.4$ km, $b = 95.6 \pm 3.0$ km, and $c = 75.6 \pm 2.3$ km; Yoder *et al.* 1989) is nearly symmetric about the spin axis, whereas the equilibrium figure is a triaxial, almost prolate,

ellipsoid. The quantitative difference between the observed and equilibrium shapes may conveniently be expressed in terms of the principal axis ratios. Observations yield $b/a = 0.96 \pm 0.04$ and $c/a = 0.76 \pm 0.03$, whereas the equilibrium figure for a satellite at Janus' distance from Saturn with a density of 0.65 g cm^{-3} is characterized by the ratios $b/a = 0.665$ and $c/a = 0.626$ (Dermott 1984, Thomas 1989). Curiously, Epimetheus, though smaller than Janus, has a figure which more closely matches the elongated equilibrium shape, although the observed axis ratios of $b/a = c/a = 0.80$ (Thomas 1989) are somewhat larger than expected.

Despite the unlikelihood of hydrostatic relaxation, it is possible that Janus' surface gravity may have significantly influenced the final stages of its accretion (or reaccretion in the quite likely event that the coorbitals represent fragments from the catastrophic disruption of a single body) by affecting the behavior of ejecta from small impacts. We may expect that preferential "downslope" movement of ejecta, combined with asymmetric slumping of crater walls, will have caused the overall shape of Janus to approach an equipotential surface. In this event, a possible explanation for Janus' nearly oblate figure is that the satellite was spinning nonsynchronously (either faster or slower) during the late stages of accretion. The average tidal field would then have the same symmetry as that imposed by rotation, but would differ in magnitude by a factor of $\frac{3}{2}(n/\Omega)^2$, where Ω is the spin angular velocity. The predicted equilibrium shape, to order e^6, is given by (Chandrasekhar 1969)

$$\left[\frac{3}{2}\left(\frac{n}{\Omega}\right)^2 + 1\right]\frac{\Omega^2}{\pi G\rho} = \frac{8}{15}(e^2 + e^4/7),$$

where the eccentricity parameter

$$e = [1 - (c/a)^2]^{1/2}.$$

For $\Omega \simeq n$, and the observed density of 0.65 g cm^{-3}, we find that $e \simeq 0.60$, corresponding to $c/a = 0.80$, which is quite close to the observed average oblateness of $2c/(a + b) = 0.78 \pm 0.04$. The major drawback to this argument would appear to be that it manifestly does not apply to Epimetheus and the F-ring shepherds, which exhibit either prolate or triaxial figures (Thomas 1989), although it is possible that the substantially greater mass of Janus is the key difference here.

As the coorbital satellites and F-ring shepherds are currently receding rapidly from the rings (Lissauer *et al.* 1985), and may in fact have accreted from ring material, it seems quite likely that other small bodies such as the Encke-gap moonlet, Pan (Showalter 1991), and perhaps large ring particles may have similarly low densities and high porosities. If the typical density of these objects is indeed $\rho_m = 0.65$ g cm^{-3}, rather than the commonly assumed value of 1.0 g cm^{-3}, then estimates of ring–satellite torques and mean ring-particle sizes may need to be revised. Furthermore, the classical Roche limit, $R_L = 2.44(\rho_p/\rho_m)^{1/3}R_p$, where R_p and ρ_p are the planet's radius and mean density, increases from 129,300 km—in the middle A ring—to 149,300 km, only 2000-km interior to the coorbitals' present location and exterior to the F ring. A consequence of this is that it is probably meaningless to speak of "equilibrium figures" for the F-ring shepherds, Prometheus and Pandora: no such equilibrium exists inside the Roche limit, at least for synchronously rotating bodies.

Of greater importance to individual ring particles, held together by cohesive forces and unlikely even to approximate ellipsoidal shapes, is the maximum distance at which small grains may be bound gravitationally to the surface of a large, spherical ring particle: $R_a = (3\rho_p/\rho_m)^{1/3}R_p = 88{,}200$ km, provocatively close to the inner edge of the B ring at 92,000 km. Inside this radius, it is expected that accretion of ring particles will be severely inhibited (Longaretti 1989). Porous, low-density ring particles are not, of course, a new concept: such a model has been proposed on the basis of collisional models for Saturn's rings by Weidenschilling *et al.* (1984), though a similar model derived by Longaretti (1989) yields near-solid densities.

5.2. *Future Observations*

Since the volume uncertainties exceed that of our mass solution, a significant reduction in the present density uncertainties of the coorbitals depends on improvements in the volume estimates. Image processing techniques which use surface landmarks or photoclinometry in addition to limb and terminator data might provide a modest improvement in shape determination for Janus and Epimetheus from analysis of the available Voyager images. Dramatic improvement (a factor greater than 2) probably must await the arrival of the Cassini spacecraft at Saturn.

The tidal acceleration of the coorbitals is of order $(-1 \times 10^{-9})°$ day^{-2}, due to ring torques. Thus we should expect a delay in longitude of $\sim$0.04° over 24 years (the interval covered by these observations), or 0.007° over the 10-year interval since the Voyager observations. Detection of this effect must probably rely on a decade-long campaign using HST instruments at their highest resolution, or on high-precision astrometry utilizing the Cassini spacecraft. However, it should be pointed out that the predicted acceleration of the inner F-ring shepherd is $(-1.3 \times 10^{-8})°$ day^{-2} (Lissauer *et al.* 1985). If we had observations of Prometheus in 1966 and 1990 similar in accuracy to the Janus measurements, this acceleration would have been near detection already. Such observa-

tions might be possible with Earth-based telescopes, utilizing active optics or clever techniques to remove the scattered-light background from the rings, and would lead to the first *direct* determination of the satellite–ring torque.

Table VI presents the evolution of ϕ with time over a quarter libration cycle ($180° \geq \phi \geq \phi_{min} = 5.64°$), or 731.714 days, as plotted in Fig. 2. Linear interpolation of this table, together with the solution parameters n_0, ϕ_0, θ, and β in Table V, will permit the prediction of Janus' and Epimetheus' mean longitudes at any past or future epoch. Corrections to true longitude, necessary for accurate work, can be made via the elliptic elements tabulated by Yoder *et al.* (1989).

The next obvious opportunity for groundbased observations is in 1995, when the Earth again crosses Saturn's ring plane and the satellites will be visible at elongation as they were in 1966 and 1980. Between 21 May and 11 August 1995 the Earth and Sun will be on opposite sides of the ring plane (Showalter *et al.* 1991), affording the best chance for detecting faint satellites. Predicted times of eastern elongation for Janus and Epimetheus on 11 August 1995, nearest the second ring-plane crossing, are 18:50 and 12:18 UT, respectively. Their mean angular separation will be $\phi = 220°$ and decreasing, as may be verified from Table VI or Fig. 2. Configurations similar to that of 1990, but with the satellites visible at superior conjunction near Saturn's south pole, will recur in November 2000 and again in December 2004, as illustrated in Fig. 15.

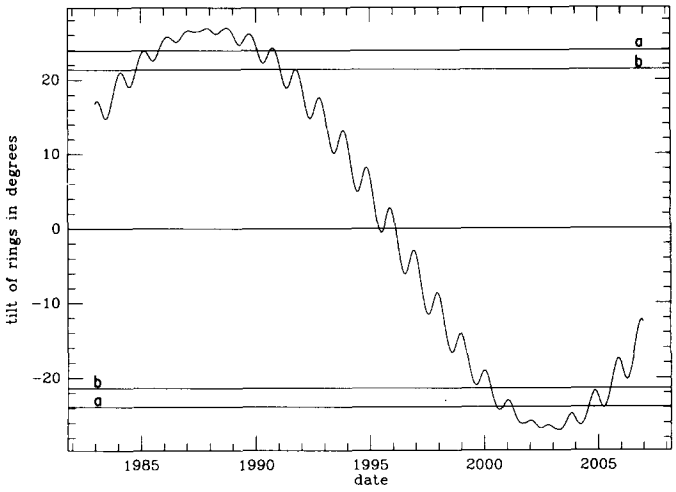

FIG. 15. Variation in the tilt of Saturn's rings, as seen from the Earth, during the period January 1983–December 2006. The lines labeled "a" and "b" indicate the narrow range within which observations such as those in July/August 1990 are possible: "a" corresponds to the complete disappearance of the A ring behind the planet at superior conjunction (23.9°) and "b" to the occultation of the coorbital satellites at conjunction (21.4°). The next opportunities at which the satellites may be observed at superior conjunction (with Saturn near opposition) occur around November 2000 and December 2004. Ring-plane crossings next occur in 1995/1996 and in September 2009.

Finally, we note that the Cassini orbiter should be well placed to monitor the close approach predicted to occur in February 2006, providing the first direct measurement of the minimum separation, as well as accurate preencounter and postencounter orbital elements.

TABLE VI
Libration Amplitude ϕ versus Time for a Quarter Libration Period

ϕ (deg)	Δ T (days)
180.00	0
167.97	50
155.92	100
143.80	150
131.61	200
119.32	250
106.93	300
94.42	350
81.80	400
69.10	450
56.35	500
43.63	550
31.10	600
19.04	650
13.47	675
8.67	700
7.18	710
6.12	720
5.64	731.714

Note. The mean longitude of either satellite can be deduced from solution 1 and this table, given that $\phi = 180°$ and $\dot{\phi} < 0$ on JD 244 4253.91549 = 15.415 January 1980, TDB. The mean longitude of Janus at this epoch was 251.4°. The full libration period is 2926.856 days, and the minimum separation in mean longitude is 5.64°.

ACKNOWLEDGMENTS

We acknowledge the able assistance of Juan Currasco at the Hale Telescope and the prompt actions by the Observatory staff in dealing with a minor mechanical emergency. Eric Persson helped with the additional observations on 11–13 July. Bob Jacobson of JPL and Don Taylor of the Royal Greenwich Observatory generously provided ephemerides for Mimas and Enceladus. Stephen Leroy of Caltech wrote the image-processing software used for all of our data reduction and produced the Saturn mosaic presented in Fig. 3. Aspects of the presentation were significantly improved by critical comments from two anonymous reviewers. This work was supported by NASA Planetary Geophysics Grants NAGW-544 and NAGW-310 at Cornell.

REFERENCES

AKSNES, K., AND F. A. FRANKLIN 1978. The evidence for faint satellites of Saturn reexamined. *Icarus* **36,** 107–118.

ALLEN, D. A. 1983. Infrared views of the giant planets. *Sky* and *Tel.* **65,** 110.

CHANDRASEKHAR, S. 1969. Ellipsoidal figures of equilibrium. Yale Univ. Press, New Haven/London.

DERMOTT, S. F. 1984. Rotation and the internal structures of the major planets and the inner satellites. *Phil. Trans. R. Soc. London A* **313,** 123–139.

DERMOTT, S. F., AND C. D. MURRAY 1981. The dynamics of tadpole and horseshoe orbits. II. The coorbital satellites of Saturn. *Icarus* **48,** 12–22.

DERMOTT, S. F., AND P. C. THOMAS 1988. The shape and internal structure of Mimas. *Icarus* **73,** 25–65.

DOLLFUS, A. 1967. Un nouveau satellite de Saturne. *C. R. Acad. Sci. Paris B* **264,** 822–824.

ELUSZKIEWICZ, J. 1990. Compaction and internal structure of Mimas. *Icarus* **84,** 215–225.

FINK, U., AND H. P. LARSON 1979. The infrared spectra of Uranus, Neptune, and Titan from 0.8 to 2.5 microns. *Astrophys. J.* **233,** 1021–1040.

FOUNTAIN, J., AND S. LARSON 1977. A new satellite of Saturn? *Science* **197,** 915–917.

FOUNTAIN, J., AND S. LARSON 1978. Saturn's ring and nearby faint satellites. *Icarus* **36,** 92–106.

HARRINGTON, R. S., AND P. K. SEIDELMANN 1981. The dynamics of the Saturnian satellites 1980S1 and 1980S3. *Icarus* **47,** 97–99.

JOHNSON, T. V., R. H. BROWN, AND J. B. POLLACK 1987. Uranus satellites: Densities and compositions. *J. Geophys. Res.* **92,** 14884–14894.

LARSON, S. M., B. A. SMITH, J. W. FOUNTAIN, AND H. J. REITSEMA 1981. The 1966 observations of the coorbiting satellites of Saturn, S10 and S11. *Icarus* **46,** 175–180.

LISSAUER, J. J., P. GOLDREICH, AND S. TREMAINE 1985. Evolution of the Janus–Epimetheus coorbital resonance due to torques from Saturn's rings. *Icarus* **64,** 425–434.

LONGARETTI, P-Y. 1989. Saturn's main ring particle size distribution: An analytic approach. *Icarus* **81,** 51–73.

MATTHEWS, K., G. NEUGEBAUER, AND P. D. NICHOLSON 1982. Maps of the rings of Uranus at a wavelength of 2.2 microns. *Icarus* **52,** 126–135.

NICHOLSON, P. D. 1984. Infrared images of the Uranian rings. In *Uranus and Neptune* (J. T. Bergstralh, Ed.), NASA CP-2330, pp. 589–608.

NICHOLSON, P. D., AND L. DONES 1991. Planetary Rings. *Rev. Geophys. Suppl.*, 313–327 (April 1991).

NICHOLSON, P. D., AND K. MATTHEWS 1991. Near-infrared observations of the Jovian ring and small satellites. *Icarus* **93,** 331–346.

NICHOLSON, P. D., AND C. C. PORCO 1988. A new constraint on Saturn's zonal gravity harmonics from Voyager observations of an eccentric ringlet. *J. Geophys. Res.* **93,** 10209–10224.

NICHOLSON, P. D., D. P. HAMILTON, K. MATTHEWS, S. S. LEROY, AND C. F. YODER 1990. New observations of Saturn's co-orbital satellites. *Bull. Am. Astron. Soc.* **22,** 1042.

NULL, G. W., E. L. LAU, E. D. BILLER, AND J. D. ANDERSON 1981. Saturn gravity results obtained from Pioneer 11 tracking data and Earth-based Saturn satellite data. *Astron. J.* **86,** 456–468.

PUETTER, R. C., AND R. W. RUSSELL 1977. The 2–4 μm spectrum of Saturn's rings. *Icarus* **32,** 37–40.

ROSEN, P. A., G. L. TYLER, E. A. MAROUF, AND J. J. LISSAUER 1991. Resonance structures in Saturn's rings probed by radio occultation. *Icarus* **93,** 25–44.

SEIDELMANN, P. K., R. S. HARRINGTON, D. PASCU, W. A. BAUM, D. G. CURRIE, J. A. WESTPHAL, AND G. E. DANIELSON 1981. Saturn satellite observations and orbits from the 1980 ring plane crossing. *Icarus* **47,** 282–287.

SHOWALTER, M. R. 1991. Visual detection of 1981S13, Saturn's eighteenth satellite, and its role in the Encke gap. *Nature* **351,** 709–713.

SHOWALTER, M. R., J. N. CUZZI, AND S. M. LARSON 1991. Structure and particle properties of Saturn's E Ring. *Icarus* **94,** 451–473.

SHU, F. H. 1984. Waves in planetary rings. In *Planetary Rings* (J. Greenberg and A. Brahic, Eds.), pp. 513–561. Univ. of Arizona Press, Tucson.

SMITH, B. A., *et al.* 1981. Encounter with Saturn: Voyager 1 imaging science results. *Science* **212,** 163–191.

SMITH, B. A., *et al.* 1982. A new look at the Saturn system: The Voyager 2 images. *Science* **215,** 504–537.

SYNNOTT, S. P., C. F. PETERS, B. A. SMITH, AND L. A. MORABITO 1981. Orbits of the small satellites of Saturn. *Science* **212,** 191–192.

TAYLOR, D. B., AND K. X. SHEN 1988. Analysis of astrometric observations from 1967 to 1983 of the major satellites of Saturn. *Astron. Astrophys.* **200,** 269–278.

THOMAS, P. C. 1989. The shapes of small satellites. *Icarus* **77,** 248–274.

VAN ALLEN, J. A. 1982. Findings on rings and inner satellites of Saturn by Pioneer 11. *Icarus* **51,** 509–527.

WALKER, R. L. 1967. *IAU Circular 1991.*

WEIDENSCHILLING, S. J., C. R. CHAPMAN, D. R. DAVIS AND R. J. GREENBERG 1984. Ring particles: Collisional interactions and physical nature. In *Planetary Rings* (J. Greenberg and A. Brahic, Eds.), pp. 367–415. Univ. of Arizona Press, Tucson.

YODER, C. F., G. COLOMBO, S. P. SYNNOTT, AND K. A. YODER 1983. Theory of motion of Saturn's coorbiting satellites. *Icarus* **53,** 431–443.

YODER, C. F., S. P. SYNNOTT, AND H. SALO 1989. Orbits and masses of Saturn's co-orbiting satellites, Janus and Epimetheus. *Astron. J.* **98,** 1875–1889.